Aalto University
School of Chemical Engineering

# Patient induced pluripotent stem cell-derived neurons as a model for a mitochondrial encephalopathy

Henriikka Vekuri

Master's program in Life Science Technologies
Biosystems and Biomaterials Engineering

Master's thesis for the degree of Master of Science in Technology
submitted for inspection, Sapporo, 1.8.2018.

| | |
|---|---|
| Supervisor | Professor Alexander Frey |
| Instructor | Riikka Äänismaa, PhD |

Aalto University
School of Chemical Engineering

| | |
|---|---|
| Author | Henriikka Vekuri |
| Title of thesis | Patient induced pluripotent stem cell-derived neurons as a model for a mitochondrial encephalopathy |
| Degree program | Life Science Technologies |
| Major | Biosystems and Biomaterials Engineering |
| Thesis supervisor | Professor Alexander Frey |
| Thesis instructor | Riikka Äänismaa, PhD |
| Date 1.8.2018 | Number of pages 50 Language English |

Abstract

In this thesis, patient induced pluripotent stem (iPS) cell-derived neurons and neural cells were used as a model for infantile onset spinocerebellar ataxia (IOSCA). IOSCA is an early-onset recessively inherited mitochondrial ataxia belonging to the Finnish disease heritage. Patients become progressively severely disabled after disease onset and currently no curative treatments exist. IOSCA is caused by a homozygous mutation (Y508C) in the mitochondrial helicase Twinkle. Twinkle participates in mitochondrial DNA (mtDNA) replication and the mutant helicase has been shown to deplete mtDNA from the brain and liver of patients. The aim of this thesis was to obtain IOSCA patient-derived neurons that would manifest a neuronal phenotype related to the disease, and analyze molecular and metabolic consequences of the mutant form of Twinkle, to shed light on the pathogenic mechanisms underlying symptoms in IOSCA.

Neuronal differentiation of iPS cells was achieved using two different methods: spontaneous differentiation as neurospheres in a suspension culture, and an adherent culture using two small molecule inhibitors blocking SMAD signaling. IOSCA patient iPS cells were able to differentiate into neurons, from here on called IOSCA neurons, using both methods. However, neuronal cultures from IOSCA cell lines differentiated as neurospheres had significantly less neurons compared to healthy controls. In addition, the patient-derived neurons were shorter and more polar, which could suggest impaired maturation.

Regardless of the differentiation method, IOSCA neurons had reduced mitochondrial networks, especially in neurites. The finding was supported by a reduction of mitochondrial respiratory chain complexes I and IV. IOSCA neural cells did not show activation of the mitochondrial integrated stress response, folate cycle or serine biosynthesis. However, untargeted metabolomics revealed that major metabolic pathways were altered in the patient-derived neural cells. Nucleotide, especially purine synthesis was clearly affected, as its intermediates comprised a significant group of decreased metabolites. Also core energy metabolic pathways were altered. IOSCA neural cells had decreased intermediates of the citric acid cycle, whereas they had accumulated medium and long-chain fatty acids. Increased levels of fatty acid synthesis intermediates suggested that the patient-derived neural cells had shifted their metabolism towards lipid synthesis, or that they were not able to utilize fatty acids that were synthesized.

Because the patient-derived neuronal cells revealed differences between patient and control cell lines, they could be further utilized to assess therapy options. The impaired nucleotide synthesis could be attempted to be alleviated through nucleotide supplementation, and remodeled energy metabolism affected through diet.

Keywords mitochondrial disease, encephalopathy, cell model, neuron, IOSCA, metabolism

Aalto University
School of Chemical Engineering

| | | |
|---|---|---|
| **Tekijä** | Henriikka Vekuri | |
| **Työn otsikko** | Potilaiden indusoiduista monikykyisistä kantasoluista erilaistetut hermosolut mallina mitokondriaaliselle aivosairaudelle | |
| **Koulutusohjelma** | Life Science Technologies | |
| **Pääaine** | Biosystems and Biomaterials Engineering | |
| **Työn valvoja** | Professori Alexander Frey | |
| **Työn ohjaaja** | Tohtori Riikka Äänismaa | |
| **Päivämäärä** 1.8.2018 | **Sivumäärä** 50 | **Kieli** Englanti |


Abstrakti

Tässä diplomityössä käytettiin potilaiden indusoiduista monikykyisistä kantasoluista erilaistettuja hermosoluja mallina IOSCA-nimiselle (Infantile onset spinocerebellar ataxia) imeväisiässä alkavalle pikkuaivo- ja selkäydinperäiselle ataksialle. IOSCA on peittyvästi periytyvä tauti, joka kuuluu suomalaiseen tautiperintöön. Potilaat ovat etenevästi vaikeavammaisia sairastumisensa jälkeen, eikä tautiin ole tällä hetkellä parantavaa hoitoa. IOSCA on mitokondriosairaus, jonka aiheuttaa homotsygoottinen mutaatio (Y508C) mitokondriaalista helikaasia Twinkleä koodaavassa geenissä. Twinkle osallistuu mitokondriaalisen DNA:n (mtDNA:n) monistamiseen ja mutaation on osoitettu johtavan mtDNA:n vähenemiseen potilaiden aivoissa ja maksassa. Tämän työn tavoitteena oli erilaistaa potilaiden indusoidut monikykyiset kantasolut hermosoluiksi, jotka ilmentäisivät tautiin liittyviä hermoston oireita, sekä analysoida mutatoituneen Twinklen aiheuttamia molekulaarisia ja aineenvaihdunnallisia muutoksia, jotta IOSCAn solutasolla vaikuttavia tautimekanismeja voitaisi ymmärtää paremmin.

Hermosolujen erilaistamiseen käytettiin kahta eri menetelmää: erilaistusta suspensiossa neurosfeereinä sekä adherenttia soluviljelmää, jossa inhiboitiin kahta merkittävää transkriptiotekijää. IOSCA-potilaiden indusoidut monikykyiset kantasolut kykenivät erilaistumaan hermosoluiksi (IOSCA-hermosoluiksi) molempia menetelmiä käyttäen. Neurosfeereinä erilaistetuissa IOSCA-hermosoluviljelmissä oli kuitenkin merkittävästi vähemmän hermosoluja verrattuna terveisiin verrokkeihin. Lisäksi nämä potilasperäiset hermosolut olivat haarautuneempia ja lyhyempiä, mikä voisi viitata siihen, että IOSCA-hermosolujen kypsyminen on puutteellista.

Riippumatta erilaistusmenetelmästä mitokondrioiden määrä oli selvästi vähentynyt IOSCA-hermosoluissa, erityisesti neuriiteissa. Tulosta vahvisti mitokondrioiden hengitysketjun proteiinikompleksien I ja IV vähentynyt määrä. IOSCA-hermosoluissa ei nähty mitokondriaalisen integroidun stressivasteen, folaattisyklin eikä seriinin biosynteesin aktivoitumista. Kohdentamaton mataboliittiprofilointi kuitenkin paljasti merkittävien aineenvaihduntapolkujen muuttuneen. Nukleotidien, erityisesti puriinien synteesi oli selvästi häiriintynyt, sillä suuri osa sen välituotteista oli merkittävästi vähentynyt. Lisäksi energia-aineenvaihdunnan keskeiset haarat olivat muuttuneet. IOSCA-hermosoluissa sitruunahappokierron välituotteet olivat huvenneet, kun taas keskipitkiä ja pitkiä rasvahappoja oli kertynyt soluihin. Lisääntyneet rasvahapposynteesin välituotteet viittasivat potilaiden hermosolujen muokanneen aineenvaihduntaansa lipidien syntetisoimiseen tai kykenemättömyyteen hyödyntää jo syntetisoituja rasvahappoja.

Koska potilaiden indusoiduista monikykyisistä kantasoluista erilaistetut hermosolut paljastivat eroja terveisiin verrokkeihin verrattuna, niitä voitaisiin tulevaisuudessa hyödyntää hoitovaihtoehtoja tutkiessa. Häiriintynyttä nukleotidien synteesiä voitaisiin mahdollisesti helpottaa nukleotidien suplementaatiolla ja energia-aineenvaihdunnan muutoksiin vaikuttaa ruokavalion kautta.



| | |
|---|---|
| Avainsanat | mitokondriotauti, aivosairaus, solumalli, hermosolu, IOSCA, aineenvaihdunta |

I would like to thank my instructor Riikka Äänismaa, PhD, for the excellent guidance throughout my master thesis journey, and Professor Anu Suomalainen-Wartiovaara for adopting a rookie into the ASW group, for the privilege to work on this project, and all the valuable comments and ideas. Thank you Professor Alexander Frey for the critical review of this thesis, which helped me improve my work. I want to thank our collaborator Dr. Nicola Zamboni for sharing his expertise in metabolomics. Thank you everyone in ASW group for the interesting discussions and all the help in the lab. Finally I would like to say a huge thank you to friends who made studying fun, and my family for the never ending support.

# Contents

# Abbreviations

AARE = Amino acid response element

ADP = Adenosine diphosphate

AMP = Adenosine monophosphate

AMPK = AMP-activated protein kinase

APP = Amyloid-beta protein

ATF = Activating transcription factor

ATP = Adenosine triphosphate

B2M = Beta-2-microglobulin

bFGF = Basic fibroblast growth factor

BH = Benjamini-Hochberg

BMP = Bone morphogenic protein

BSA = Bovine serum albumin

CI = NADH dehydrogenase

CII = Succinate dehydrogenase

CIII = Coenzyme Q10-cytochrome c oxidoreductase

CIV = Cytochrome c oxidase

CNS = Central nervous system

CV = ATP synthase

CoA = Coenzyme A

CSF = Cerebrospinal fluid

CytB = Cytochrome B

DAPI = 4',6-diamidino-2-phenylindole

dGUOK = Deoxyguanosine kinase

D-loop = Displacement-loop

DNA = Deoxyribonucleic acid

dNDP = Deoxyribonucleotide diphosphate

dNMP = Deoxyribonucleotide monophosphate

dNTP = Deoxyribonucleotide triphosphate

DRP1 = Dynamin-related protein 1

EDTA = Ethylenediaminetetraacetic acid

ER = Endoplasmic reticulum

ES cell = Emryonic stem cell

ETC = Electron transport chain

FAD = Flavin adenine dinucleotide

FAO = Fatty acid oxidation

FGF21 = Fibroblast growth factor 21

GDP = Guanosine diphosphate

GMP = Guanosine monophosphate

GTP = Guanosine triphosphate

IOSCA = Infantile onset spinocerebellar ataxia

iPS cell = Induced pluripotent stem cell

ISR = Integrated stress response

ISRmt= Integrated mitochondrial stress response

MAP2 = Microtubule associated protein 2

MCAD = Medium-chain acyl-CoA dehydrogenase

MDS = Mitochondrial DNA depletion syndrome

MPV17 = Mitochondrial inner membrane protein 17

mtDNA = Mitochondrial DNA

MTHFD2 = Methylene-tetrahydrofolate dehydrogenase 2

mTORC1 = Mechanistic target of rapamycin complex 1

NAA = N-acetyl-L-aspartic acid

NAD = Nicotinamide adenine dinucleotide

NADP = Nicotinamide adenine dinucleotide phosphate

NDM = Neural differentiation medium

NPC = Neural progenitor cell

NTP =Nucleoside triphosphate

OPA1 = Optic atrophy 1

OXPHOS = Oxidative phosphorylation

PAX6 = Paired box protein 6

PB = Phosphate buffer

PBS = Phosphate-buffered saline

PHGDH = Phosphoglycerate dehydrogenase

PLS-DA = Partial least squares discriminant analysis

PNS = Peripheral nervous system

PolG = Polymerase gamma

PRPP = 5-phosphoribosyl-$\alpha$-1-pyrophosphate

PSAT1 = Phosphoserine aminotransferase 1

RITOLS = RNA incorporated throughout the lagging strand

RNA = Ribonucleic acid

RNR = Ribonucleotide reductase

ROS = Reactive oxygen species

RRM2B = Ribonucleotide-diphosphate reductase subunit M2

SUCLA2 = Succinate-CoA ligase ADP-forming subunit beta

SUCLG1 = Succinate Co-A ligase ADP/GDP forming subunit alpha

SSBP1 = Single stranded DNA binding protein 1

TCA cycle = Tricarbocylic acid cycle

TFAM = Mitochondrial transcription factor A

TGF-$\beta$ = Transforming growth factor $\beta$

TK1 = Thymidine kinase 1

TK2 = Thymidine kinase 2

TOM20 = Translocase of outer membrane 20

TRIB3 = Tribbles homologue 3

tRNA = Transfer RNA

TYMP = Thymidine phosphorylase

UMP = Uridine monophosphate

# 1 Introduction

Mitochondrial diseases can be caused either by mutations in nuclear encoded or mitochondrial DNA eventually disrupting mitochondrial function. They are the most common inherited metabolic diseases, usually manifesting in tissues and organs that require most energy, such as the nervous system, muscle, liver and heart. However, age of onset varies from infancy to old age and practically any tissue of the body can be affected. Also the inheritance pattern can be any: maternally inherited, autosomal dominant, recessive or X-linked. Mutations can also occur *de novo* during embryogenesis. Currently therapy focuses on relieving symptoms and no curative treatments are available. Because of the heterogeneity of mitochondrial diseases, making diagnoses can be difficult. It is mainly based on biochemical analyses, magnetic resonance imaging, tissue biopsy samples and increasingly, genetic testing. (Nunnari and Suomalainen, 2012)

Impaired maintenance of mitochondrial DNA can lead to mitochondrial DNA (mtDNA) depletion or deletions, and is a major cause of mitochondrial diseases. Because neurons critically depend on mitochondrial function due to their extremely high energy demand and special morphology, mitochondrial dysfunction often leads to neurodegeneration. Mitochondria are mainly known for generating adenosine triphosphate (ATP), the energy currency used by all cell types. Besides being cellular powerhouses, mitochondria take part in many important processes, such as biosynthetic pathways, $Ca^{2+}$-signaling, cell cycle control and apoptosis. Therefore, mitochondrial dysfunction does not necessarily lead to an inadequate amount of ATP, but rather it can initiate an integrated stress response, alter metabolic pathways or cause an imbalance in redox balance. (Suomalainen and Battersby, 2017)

Human diseases are often studied using animals as a model. However, they do not always recapitulate the disease phenotype and require extensive resources in time and money. Therefore, cellular models can be used as an alternative and additional method. When a disease affects the nervous system, a tissue biopsy is not desirable or even applicable. Induced pluripotent stem (iPS) cells are obtained from differentiated cells, such as skin fibroblasts, by genetically engineering them back to a stem cell state where they hold the capacity to differentiate into all three germ layers (Takahashi and Yamanaka, 2006). Therefore, neurons derived from patient iPS cells make an excellent tool for studying molecular mechanisms of neuropathological diseases *in vitro*.

The aim of this thesis was to study an early onset severely disabling mitochondrial ataxia, infantile onset spinocerebellar ataxia (IOSCA), using patient iPS cell-derived neurons and neural cells as a model. IOSCA is a recessively inherited disease which belongs to the Finnish disease heritage with a carrier frequency of more than 1:230 (Hakonen et al., 2008). IOSCA is caused by a homozygous mutation (Y508C) in the mitochondrial helicase Twinkle (Nikali et al., 2005). Symptoms start to manifest during infancy and include progressive spinocerebellar ataxia, hearing loss, epilepsy and hepatopathy (Koskinen et al., 1994). IOSCA patients develop mitochondrial DNA depletion in brain and liver (Hakonen et al., 2008), and the disease has been shown to alter major metabolic pathways through one-carbon metabolism (Nikkanen et al., 2016). Currently there is no curative treatment available and identification of the underlying molecular mechanisms is essential to enable intervention.

# 2 Mitochondria

## 2.1 Dynamic networks of bacterial descendants

Mitochondria are the organelles that convert energy from carbohydrates, fatty acids and proteins to adenosine triphosphate (ATP), the energy currency of all cells. Mitochondria originate from an alpha-proteobacterium that once was engulfed by an early eukaryote (Lane and Martin, 2010). All human cells except mature red blood cells contain mitochondria, but the number varies in different tissues depending on energy requirements. Mitochondria consist of an outer membrane facing the cytosol and a highly folded inner membrane separating two compartments: the intermembrane space and the mitochondrial matrix (figure 1). Both membranes are phospholipid bilayers embedded with proteins. The outer membrane covers the entire organelle and is numerous with pores that ions and small molecules, even proteins, are able to pass. The inner membrane is much more impermeable and loaded with proteins involved in energy metabolism. It is arranged into highly folded cristae which increases the surface area greatly.

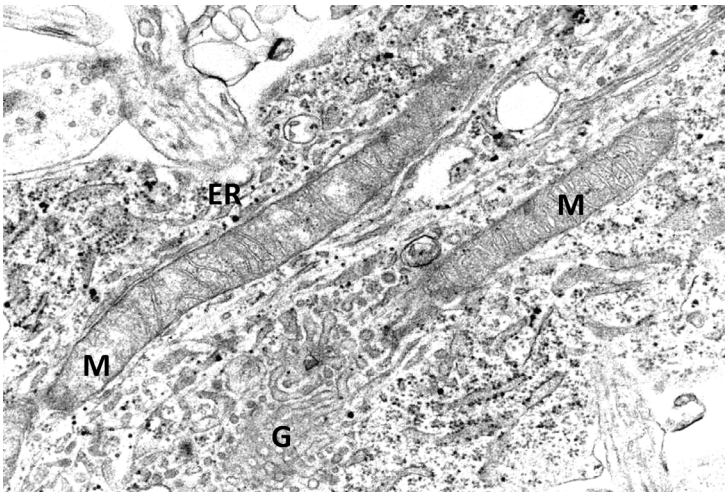


Figure 1: A transmission electron microscope image of mitochondria in iPS cell-derived neurons. M = mitochondrion, G = golgi apparatus, ER = endoplasmic reticulum. Imaging by Christopher Jackson.

Mitochondria constantly participate in fission and fusion events and form a highly dynamic network that is integrated to other cellular compartments such as the endoplasmic reticulum (ER) (figure 1). Mitochondria move along microtubules and alter their network structure to meet the demands of the changing cellular environment. Mitochondrial dynamics allows the exchange of mitochondrial contents and lipids throughout the mitochondrial population. Fusion alleviates stress as contents of partially damaged mitochondria are mixed. Fission creates new mitochondria and enables the isolation of damaged ones. Several proteins control mitochondrial dynamics. Two proteins are involved in the fusion of outer mitochondrial membranes: Mitofusin 1 and 2, and one in the fusion of inner membranes: OPA1 (Optic atrophy 1) (Song et al., 2009). Mitochondrial fission occurs at sites where mitochondria contact ER tubules, and DRP1 (Dynamin-related protein 1) is recruited to perform fission (Smirnova et al., 2001; Friedman et al., 2011). (Chen and Chan, 2009)

The unique origin of mitochondria and the fact that they participate in so many vital processes make mitochondria particularly vulnerable to accumulating damage throughout life. Therefore, specific mitochondrial quality control systems have evolved to ensure mitochondrial integrity. First of all, mitochondria are loaded with proteases and chaperones that protect them from accumulating misfolded proteins (Rugarli and Langer, 2012). Mitochondrial quality is managed also on an organellar level. During stress, mitochondria hyperfuse to increase ATP production and avoid autophagy (Rugarli and Langer, 2012). In case mitochondrial fusion is impaired due to mitochondrial dysfunction, continuous fission events fragment the mitochondrial network. Mitochondrial fragmentation signals for mitochondrial turnover and fragmented mitochondria are removed through selective autophagy, or mitophagy. In the process of mitophagy, mitochondria are engulfed into autophagosome marker microtubule associated protein 1 light chain 3 (LC3) coated vesicles and trafficked to the lysosome for degradation (figure 2) (Kim et al., 2007).

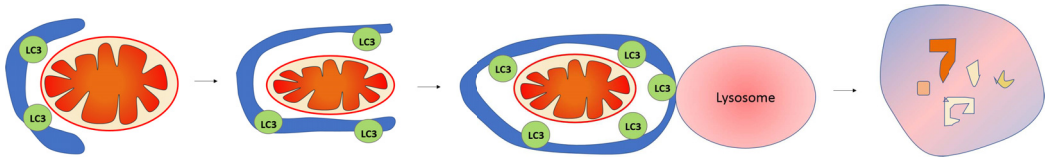


Figure 2: Mitophagy is the controlled process of identifying, isolating and trafficking mitochondria to the lysosome for degradation in autophagosome marker microtubule associated protein 1 light chain 3 (LC3) coated vesicles.

## 2.2 Own genome with a distinct translation and maintenance machinery

Mitochondria contain their own DNA which encodes for 13 of the total 93 protein subunits of the respiratory chain and ATP synthase, as well as 22 transfer and 2 ribosomal RNAs involved in their translation (figure 3). Mitochondrial DNA is almost exclusively maternally inherited in all mammals. Mitochondria contain multiple copies of the double-stranded circular 16 569 base pair long mtDNA molecule (Anderson et al., 1981), with the exact number commonly being 2-10, at least in cultured cells (Iborra et al., 2004). The outer strand contains most mitochondrial genes and is referred to as the heavy strand (H-strand). The inner strand is named the light strand (L-strand). The displacement loop, or D-loop, is a major control region for mtDNA expression as it contains major promoters and the origin of replication for the leading strand. Physically it is a short strand corresponding to the L-strand and displacing the H-strand.

Mitochondrial DNA is located within the mitochondrial matrix and organized into protein containing nucleoids that are attached to the inner mitochondrial membrane. Mitochondrial DNA and its translation machinery still present features of the prokaryotic origin. The genetic code of four codons differs from eukaryotic genomes and mitochondrial ribosomal RNAs resemble more bacterial than eukaryotic ones. The mitochondrial genome is very compact as it does not contain introns. It has decreased in size throughout evolution due to gene transfer to the nucleus (Timmis et al., 2004). Therefore, mitochondria are under control of two distinct genomes. The vast majority of mitochondrial proteins are encoded in

the nucleus, translated in the cytosol and imported to mitochondria through specialized transporters (Neupert and Herrmann, 2007).

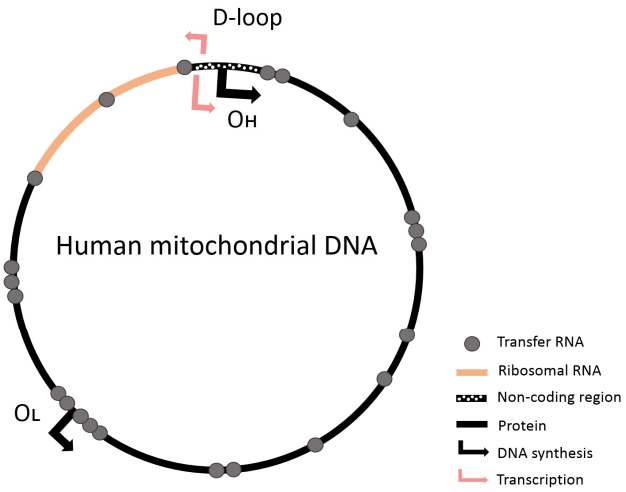


Figure 3: Map of the mitochondrial genome. The outer strand contains most mitochondrial genes and is called the heavy strand, whereas the inner strand is referred to as the light strand. D-loop (displacement-loop) = a major control region for mitochondrial DNA expression. $O_H$ and $O_L$ = origin of replication for each strand.

The exact mechanism of mtDNA replication is still under some debate. The strand-displacement model suggests that mtDNA is replicated unidirectionally starting from the D-loop, until the origin of replication for the light strand is reached, and then the light strand replicated to the opposite direction (Clayton, 1982). Another model proposes that mtDNA is replicated bidirectionally in a strand-coupled manner, starting from a wider region downstream of the origin of replication for the heavy strand (Holt et al., 2000). Finally, the RITOLS (RNA incorporated throughout the lagging strand) model predicts unidirectional synthesis but while DNA synthesis progresses on the leading strand, RNA is incorporated on the lagging strand, and as DNA is synthesized on the lagging strand, RNA is replaced by DNA (Yang et al., 2002; Yasukawa et al., 2006). However, there is evidence of different replication models occurring in different tissues and also between different species (Pohjoismaki et al., 2009). Unlike nuclear DNA replication, mtDNA replication is not linked to cell cycle but instead mitochondrial fission, which is regulated by ER-mitochondria contacts, at least in cultured cells (Clayton, 1982; Lewis et al., 2016).

The entire mitochondrial DNA maintenance machinery is encoded in the nucleus. Mitochondrial DNA is replicated by mitochondrial DNA polymerase gamma (PolG), the replicative helicase Twinkle, mitochondrial single-stranded DNA binding protein (SSBP1), mitochondrial RNA polymerase, mitochondrial transcription factor A (TFAM) and some additional mtDNA processing enzymes (figure 4). The minimal replisome consists of PolG, Twinkle and SSBP1 (Korhonen et al., 2004).

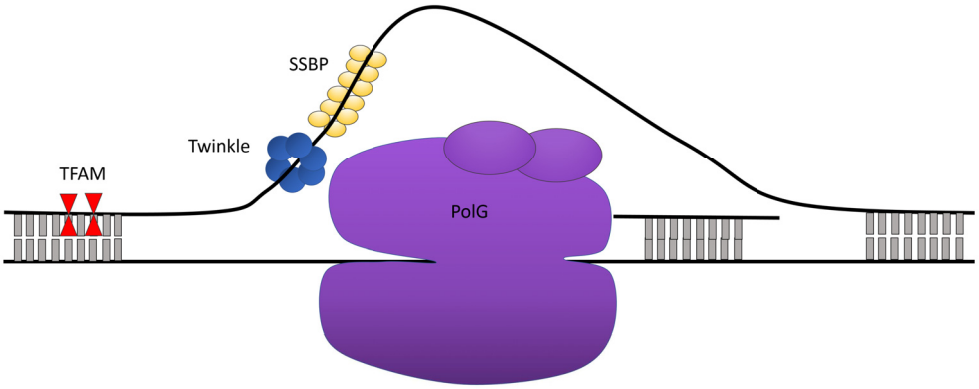


Figure 4: The minimal mitochondrial replisome consists of polymerase gamma (PolG), the helicase Twinkle and single-stranded DNA binding protein (SSBP). Mitochondrial transcription factor A (TFAM) is one regulator of mtDNA copy number.

TFAM is a transcription factor that bends and unwinds mitochondrial DNA, and is necessary for mtDNA expression (Fisher et al., 1992; Shi et al., 2012a). TFAM has been shown to also act as a regulator of mtDNA copy number (Ekstrand et al., 2004). It is the most abundant protein in nucleoids and therefore a critical factor in packaging mtDNA. PolG is the main mitochondrial DNA polymerase and vital for mtDNA replication. It is a heterotrimeric protein which consists of one catalytic subunit (PolG) and two regulatory subunits (PolG2) (Yakubovskaya et al., 2006). Mitochondrial DNA is replicated with high fidelity due to the exonuclease proofreading activity of PolG (Longley et al., 1998). Twinkle is the mitochondrial helicase that has a hexameric ring-like structure homologous to the phage T7 primase/helicase (Spelbrink et al., 2001). Twinkle has lost its primase activity but still unwinds mitochondrial DNA for replication, and probably acts as a licensing factor, since overexpression of Twinkle increases mtDNA copy number (Tyynismaa et al., 2004). However, the exact mechanism of mtDNA copy number control is unknown.

## 2.3 Mitochondria is the powerhouse of the cell

Mitochondria are key players in energy metabolism which is reflected by the fact that an increase in the demand of ATP leads to increased mitochondrial mass (Hoppeler and Fluck, 2003). Mitochondria generate ATP through three main pathways: oxidative phosphorylation (OXPHOS), the tricarboxylic acid cycle (TCA cycle) and fatty acid oxidation (FAO), which all operate in the mitochondrial matrix. The tricarboxylic acid cycle is an important driver of cellular respiration, harvesting energy from acetyl coenzyme A (acetyl-CoA) to the reducing equivalents NADH (nicotinamide adenine dinucleotide) and $FADH_2$ (flavin adenine dinucleotide). Fatty acid oxidation breaks down fatty acids and generates acetyl-CoA, which enters the TCA cycle, and also NADH and $FADH_2$. The electron carriers pass their electrons to the mitochondrial electron transport chain (ETC), which generates most ATP in cellular respiration through oxidative phosphorylation. Mitochondrial energy metabolism is summarized in figure 5.

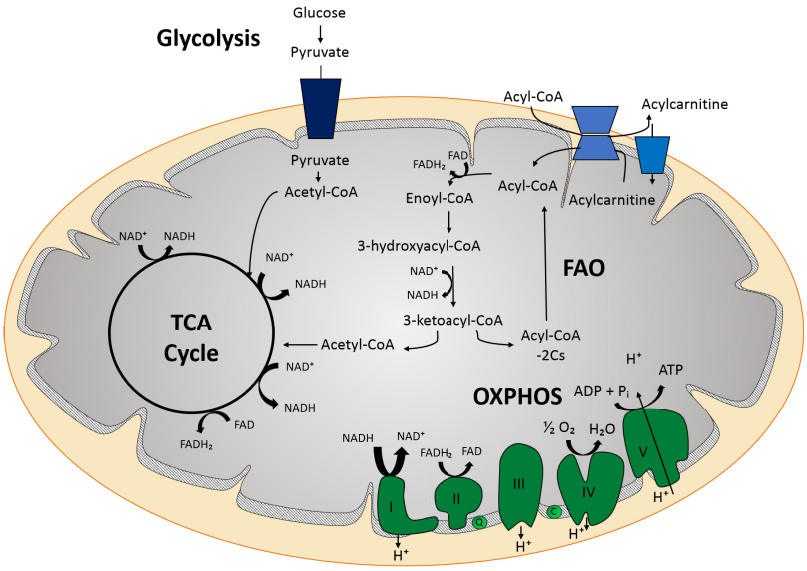


Figure 5: Mitochondria generate ATP through three main pathways: fatty acid oxidation (FAO), the tricarboxylic acid cycle (TCA cycle) and oxidative phosphorylation (OXPHOS).

Mitochondrial activity is sensed through $NAD^+$/NADH and AMP/ATP ratios, as well as acetyl-CoA levels. Sensors include transcription factors, hormones, cofactors, nuclear receptors and kinases (Nunnari and Suomalainen, 2012). An increased AMP/ATP ratio or ADP concentration, indicating insufficient mitochondrial function, is sensed by AMP-activated protein kinase (AMPK) (Carling et al., 1987; Hardie et al., 2006). AMPK activation leads to upregulation of catabolic processes, OXPHOS and autophagy, whereas cell growth and proliferation are downregulated (Carling et al., 2011). Another key metabolic sensor is Sirtuin 1, which responds to an increase in $NAD^+$-levels. Together with AMPK it regulates mitochondrial biogenesis and ATP production via the transcription cofactor peroxisome proliferator-activated receptor gamma coactivator 1 alpha (Canto et al., 2010; Wu et al., 1999).

### 2.3.1 The tricarboxylic acid cycle

Carbohydrates, fats and amino acids are initially processed to acetyl coenzyme A which then enters the TCA cycle that operates in the mitochondrial matrix. Acetyl-CoA can be derived from glycolysis, pyruvate oxidation or fatty acid oxidation. The TCA cycle can also be fed by some amino acids. The TCA cycle consists of eight enzyme-catalyzed reactions that while oxidizing acetyl-CoA, reduce $NAD^+$ to NADH, and FAD to $FADH_2$. NADH and $FADH_2$ act as electron carriers and transfer their electrons to the electron transport chain; NADH to complex I and $FADH_2$ to complex II.

### 2.3.2 Fatty acid oxidation

Fatty acids are a major source of energy that are required especially during fasting and long term exercise. Short- and medium-chain fatty acids are able to passively diffuse cell membranes but long-chain fatty acids need to be transported by sodium dependent fatty acid transporters (Hirsch et al., 1998). Once inside cells, fatty acids are activated by converting them to fatty acyl-CoA esters by fatty acyl-CoA-synthetases. Fatty acyl-CoA esters can serve as substrates for cholesterol, phospholipids and triacylglycerol, or be transported to mitochondria for FAO by the carnitine shuttle.

Fatty acid oxidation occurs as a series of dehydrogenation, hydration, a second dehydrogenation and thiolysis reactions. The end product of each cycle is a fatty acyl-CoA ester shortened by two carbons, an acetyl-CoA molecule and two electrons that proceed to OXPHOS. The shortened fatty acyl-CoA ester enters the cycle repeatedly until only two acetyl-CoAs remain. In mammals fatty acid oxidation requires also peroxisomes. Long- and medium-chain fatty acids can be oxidized by both mitochondria and peroxisomes, however, long-chain dicarboxylic, very long-chain monocarboxylic and branched-chain fatty acids are only accepted by peroxisomes.

### 2.3.3 Oxidative phosphorylation

Most energy in mammalian cells is produced in the aerobic process of oxidative phosphorylation by the mitochondrial electron transport chain. The ETC consists of four protein complexes located on the inner mitochondrial membrane: complex I (NADH dehydrogenase), complex II (succinate dehydrogenase), complex III (coenzyme Q10-cytochrome c oxidoreductase) and complex IV (cytochrome c oxidase), and ATP synthase, which is often referred to as complex V. CI accepts electrons from NADH yielding $NAD^+$. CII accepts electrons from $FADH_2$ yielding FAD, and operates also in the TCA cycle converting succinate to fumarate. Both CI and CII donate the electrons to the small mobile coenzyme Q10 (CoQ10 or ubiquinone) which is reduced to ubiquinol. $NAD^+$ and FAD are recycled back to the TCA cycle. Ubiquinol travels through the membrane carrying the electrons to complex III that transfers them to cytochrome c. In the last step, CIV donates the electrons from cytochrome c to molecular oxygen thereby forming water. Importantly, CI, CIII and CIV pump protons from the mitochondrial matrix to the intermembrane space while transferring electrons to each other, and thus create an electrochemical potential across the membrane (Mitchell, 1961). As protons move back to the mitochondrial matrix along the electrochemical gradient through ATP synthase, ADP is phosphorylated to ATP. The respiratory chain complexes form combinations of supercomplexes or respirasomes that are physically and functionally linked, which enhances the transfer of electrons (Schagger and Pfeiffer, 2000). (Saraste, 1999) Figure 6 gives an overview of the process of oxidative phosphorylation.

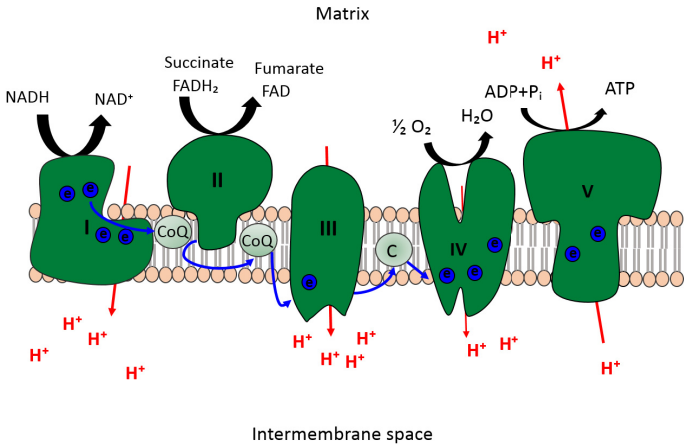


Figure 6: The mitochondrial electron transport chain consists of four protein complexes that shuttle electrons to one and other and finally donate them to oxygen. Simultaneously CI, III and IV pump protons to the intermembrane space from the mitochondrial matrix. As protons travel back to the matrix through ATP synthase, or CV, ADP is phosphorylated to ATP.

## 2.4 Mitochondria are chemical factories and signaling centers

Although mitochondria are most known for generating ATP, they have numerous other crucial functions. Mitochondria regulate pools of metabolites, amino acids and cofactors for several regulatory enzymes (Suomalainen and Battersby, 2017). They also have a central role in synthesizing heme for oxygen delivery and iron-sulfur clusters for metalloproteins including those of the respiratory chain (Lill and Kispal, 2000). Mitochondria are closely connected to the endoplasmic reticulum and the ER-mitochondrial junction is important for calcium homeostasis and signaling (Csordas et al., 2010). Mitochondrial intermediate metabolites can act as epigenetic regulators in the nucleus, and control cell cycle and apoptosis (Lu and Thompson, 2012). A functional electron transport chain maintains an electrochemical gradient across the mitochondrial inner membrane which is important for more than just ATP production. It is needed for example for protein import (Dudek et al., 2013) and changes in the membrane potential signal of mitochondrial dysfunction. Mitochondrial depolarization causes degradation of OPA1 and mitofusins and therefore mitochondrial fragmentation (Rugarli and Langer, 2012).

Mitochondria are also at the core of the folate cycle which is tightly linked to a larger set of physiological processes known as one-carbon metabolism. The folate cycle produces formyl-methionine for mitochondrial translation initiation and folates that activate and transfer one-carbon units to purine synthesis, methyl cycle and transsulfuration in the cytoplasm (Tibbetts and Appling, 2010). One-carbon metabolism supports amino acid homeostasis of glycine, serine and methionine, epigenetic maintenance as well as redox defense (Ducker and Rabinowitz, 2017). Mitochondrial 5,10-methylene-tetrahydrofolate dehydrogenase produces NADH when active, and therefore connects one-carbon metabolism to the respiratory state of the cell. Interestingly, mitochondrial DNA replication defects have been shown to remodel one-carbon metabolism (Nikkanen et al., 2016). A graphical overview of one-carbon metabolism is presented in figure 7.

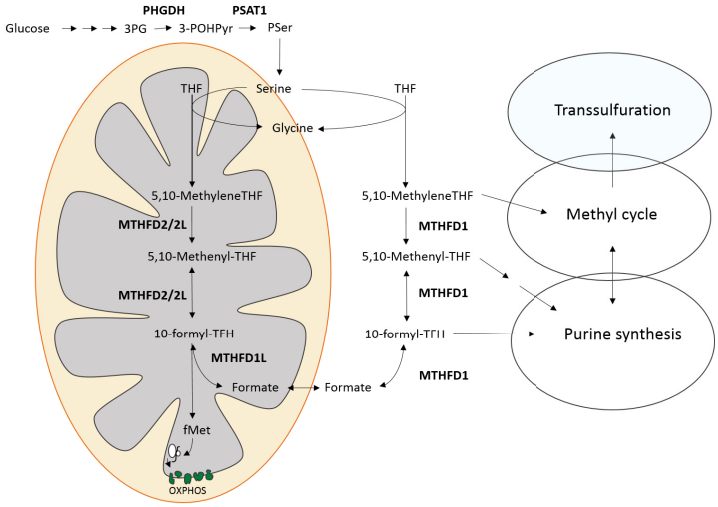


Figure 7: Mitochondria are at the core of one-carbon metabolism, which supports a group of important cytoplasmic processes: purine synthesis, methyl cycle and transsulfuration. PHGDG = phosphoglycerate dehydrogenase, PSAT1 = phosphoserine aminotransferase 1, 3PG = 3-phosphoglycerate, 3-POHPyr = 3-phosphohydroxypuryvate, PSer = phosphoserine, THF = tetrahydrofolate, MTHFD = methylene-tetrahydrofolate dehydrogenase, fMet = formyl methionine.

## 2.5 Neurons are demanding habitats for mitochondria

The brain requires 20% of the total oxygen supply of the body (Kann and Kovacs, 2007). Neurons alone require immense amounts of ATP for maintaining ion gradients across their membranes and for neurotransmission. They are also highly polarized post-mitotic cells with far-reaching extensions, which causes special requirements regarding for example membrane maintenance and axonal transport. Mitochondria need to form a highly mobile network in neurons and rely on anterograde and retrograde transport to areas of high energy demand, such as synapses and growth cones seeking for synaptic targets. Therefore, neurons critically depend on reliable mitochondrial function.

Mitochondrial fusion and axonal transport machineries are tightly connected. Mutations in OPA1 cause optic atrophy (Delettre et al., 2000) and mutations in Mitofusin 2 a peripheral neuropathy: Charcot-Marie-Tooth type 2A (Zuchner et al., 2004). Therefore, it is clear that neurons require intact mitochondrial dynamics. Changes in mitochondrial morphology also disrupt interactions with the endoplasmic reticulum and therefore mitochondrial $Ca^{2+}$-homeostasis. A tight regulation of calcium buffering in synapses is crucial for neuronal firing and an excessive influx of calcium can initiate apoptosis (Giorgi et al., 2008). Mitochondria also supply building blocks for neurotransmitters and are involved in lipid synthesis which is crucial for neuronal function (Kann and Kovacs, 2007).

In neurons, mitochondria need to be transported from the cell body to neurites that can be even over a meter long. With a velocity ranging from 0.1$\mu$m/sec to 2$\mu$m/sec (Ligon and Steward, 2000), it could take two weeks for a mitochondrion to reach the synapse after leaving from the soma. Therefore, their half life in neurons is longer than that of mitochondria in other tissues. In rat brain their half life has been found to exceed four weeks (Menzies and Gold, 1971), so in human brain their half life could

reach months. Most nuclear encoded mitochondrial proteins are loaded to mitochondria in the cell body before they travel to their destination. Thus, besides being vulnerable of accumulating damage, neuronal mitochondria face a risk of being outdated when arriving to their destination. Also autophagosomes, although being formed in axons, have to travel a long distance to the cell body to fuse with lysosomes (Rugarli and Langer, 2012). It is not known, how this process is affected by mitochondrial dysfunction.

# 3 Consequences of mitochondrial dysfunction

## 3.1 Mitochondrial DNA depletion syndromes

Mitochondrial DNA depletion syndromes (MDS) are caused by loss of mtDNA. Mitochondrial DNA maintenance can be challenged due to an impaired mtDNA replication machinery or an insufficient amount of necessary building blocks: dNTPs (deoxyribonucleoside triphosphates). Mitochondrial DNA depletion syndromes typically manifest at infancy with high tissue specificity leading to impaired OXPHOS in affected tissues and organs. Energy metabolism is mainly glycolytic during fetal life so even severe respiratory deficiencies may not prevent normal development. After birth, the role of oxidative energy metabolism increases, as does the amount of mtDNA and expression of its proteins targeted to the respiratory chain. MDS are clinically heterogeneous but usually they can be categorized into either myopathic, hepatocerebral, encephalomyopathic or neurogastrointestinal forms. Mitochondrial DNA depletion syndromes often lead to early death. (Suomalainen and Isohanni, 2010)

The genetic background of mitochondrial DNA depletion syndromes is heterogeneous. Most MDS causing mutations affect proteins involved in dNTP synthesis. The cytosolic nucleotide pools are closely linked to mitochondrial ones and in post-mitotic tissues they mainly serve mtDNA replication. Myopathic MDS is caused by mutations in TK2 (thymidine kinase 2) which operates inside mitochondria in the pyrimidine nucleoside salvage pathway. Encephalomyopathic forms are caused by mutations in RRM2B (ribonucleoside-diphosphate reductase subunit M2), SUCLA2 (succinate-CoA ligase ADP-forming beta subunit) and SUCLG1 (mitochondrial succinate-CoA ligase ADP/GDP-forming subunit alpha). RRM2B encodes the small subunit of the cytosolic ribonucleotide reductase, which catalyzes the reduction of ribonucleoside diphosphates into their corresponding deoxyribonucleoside diphosphates. Succinyl-CoA ligase is a TCA cycle enzyme catalyzing the reversible conversion of succinyl-CoA to succinate, and ADP to ATP or GDP to GTP, depending on its beta-subunit. Hepatocerebral forms of MDS are caused by mutations in dGUOK (deoxyguanosine kinase) which is involved in the mitochondrial purine nucleoside salvage pathway, MPV17 (mitochondrial inner membrane protein 17) with an unknown role in mtDNA maintenance, and PolG and Twinkle which belong to the mtDNA replication fork. Mutations in TYMP (thymidine phosphorylase) cause a mitochondrial neurogastrointestinal encephalopathy. TYMP encodes thymidine phosphorylase that catalyzes the conversion of thymidine to thymine and deoxyuridine to uracil in the cytosol. Figure 8 gives an overview of nucleotide synthesis and illustrates proteins that have been identified to cause mitochondrial DNA depletion syndromes. (Suomalainen and Isohanni, 2010)

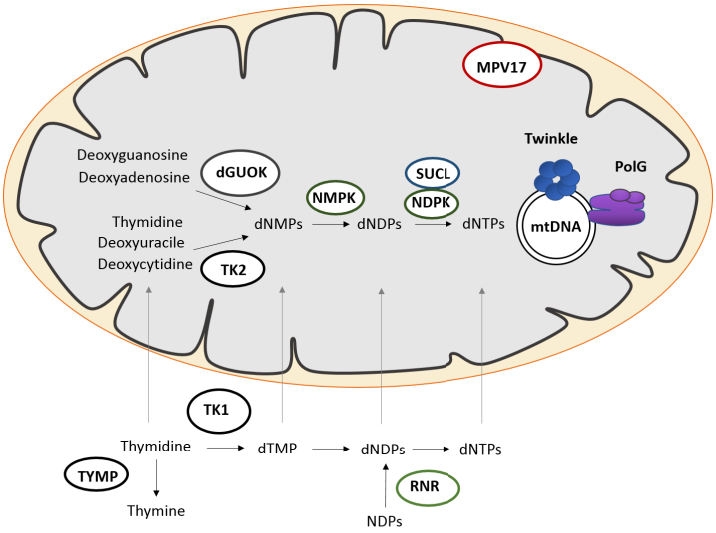


Figure 8: Mitochondrial DNA depletion syndromes are caused by mutations impairing nucleotide synthesis (TK2 = thymidine kinase 2, dGUOK = deoxyguanosine kinase, RNR = ribonucleotide reductase, SUCL = succinyl-CoA ligase, TYMP = thymidine phosphorylase) or mtDNA replication (PolG = polymerase gamma, Twinkle). Also mutations in mitochondrial inner membrane protein 17 (MPV17), with an unknown function, cause MDS. NDPK = nucleoside diphosphate kinase, NMPK = nucleoside monophosphate kinase, TK1 = thymidine kinase 1, dNTP = deoxynucleotide triphosphate, dNDP = deoxynucleotide diphosphate, dNMP = deoxynucleotide monophosphate.

Puzzling is that even the most severe forms of MDS do not cause developmental abnormalities even though fetal life is highly proliferative and requires active mtDNA replication. This could be explained by maternal contribution to the fetal dNTP pools or a high expression of defective proteins during fetal life. Apart from MDS caused by mutations in SUCLA2, the manifestation of mitochondrial DNA depletion syndromes is different from Leigh syndrome, which is caused by deficiencies in one or more of the respiratory chain protein complexes and their assembly factors. PolG related phenotypes include mitochondrial recessive ataxia syndrome (MIRAS) which closely resembles IOSCA, Alpers syndrome and sensory ataxia, neuropathy, dysarthria, ophthalmoplegia (SANDO) syndrome. In addition to IOSCA, mutations in Twinkle have been associated with autosomal dominant progressive ophthalmoplegia. Only PolG and Twinkle defects cause intractable epilepsy and both are also associated with liver failure induced by the epilepsy drug valproate. (El-Hattab and Scaglia, 2013; Suomalainen and Isohanni, 2010)

### 3.1.1 Infantile onset spinocerebellar ataxia

Infantile onset spinocerebellar ataxia is a recessively inherited mitochondrial ataxia belonging to Finnish disease heritage with a carrier frequency of more than 1:230 (Hakonen et al., 2008). IOSCA is caused by a homozygous (Y508C) mutation in the mitochondrial helicase Twinkle (Nikali et al., 2005). The mutation has been also found as compound heterozygous with the mutation A318T, in patients manifesting an Alpers-like hepatocerebral disease (Hakonen et al., 2007). IOSCA patients develop normally until the age of 10 to 18 months when first symptoms of ataxia, dysarthria, hypotonia, hearing loss and

ophthalmoplegia start to present. Spinocerebellar degeneration is progressive; neuropathological features include atrophy of the cerebellum, brain stem and spinal cord, as well as sensory axonal neuropathy. Based on examinations on the sural nerve, myelinated fibers degenerate progressively and large myelinated fibers are completely lost. Patients require a wheelchair or a walker by adolescence and hearing loss progresses into deafness. A difficult-to-treat epilepsy starts usually in teenage and often develops into a life threatening status epilepticus. Additional clinical characteristics include migraine, optic atrophy, female hypergonadotropic hypogonadism and liver involvement. (Koskinen et al., 1994) Currently the underlying molecular mechanisms of the disease are unknown and there is no curative treatment.

The Y508C mutation is located in the helicase domain of Twinkle. Homology modeling of the mutant protein has revealed that the mutation uncouples nucleoside triphosphate (NTP) hydrolysis from the binding and translocation of single-stranded DNA resulting in independent NTP hydrolysis (Nikkanen et al., 2016). IOSCA patients develop mtDNA depletion in large neurons and liver, but no mtDNA deletions. The IOSCA mutation also creates a conserved heme-binding motif but it does not bind heme covalently. The disease affects especially large neurons of the frontal cortex and cerebellum, and in line with mtDNA depletion, respiratory chain complex I, and more subtly also complex IV, are reduced. Post mortem analysis of the brain has also revealed a loss of Purkinje cells in the cerebellum as well as gliosis and atrophy of the dentate nucleus. (Hakonen et al., 2008)

Standard laboratory metabolic screenings, including cerebrospinal fluid (CSF) lactate, have been normal in IOSCA patients (Koskinen et al., 1994). Patients with compound heterozygous mutations (Y508C and A318T) however, have had mildly elevated serum and CSF lactate, and occasionally elevated liver transaminases and alpha-fetoprotein (Hakonen et al., 2007). However, a 100 metabolite analysis of IOSCA patient blood revealed remodeling of one-carbon metabolism (Nikkanen et al., 2016). The main end products of transsulfuration were decreased and also purine metabolism was affected as adenosine was decreased almost 8-fold in IOSCA patient blood compared to controls (Nikkanen et al., 2016). Also guanidinoacetate/creatine metabolism was disturbed (Nikkanen et al., 2016). An IOSCA patient and a heat map of 25 most significantly altered metabolites in IOSCA patient blood is shown in figure 9.

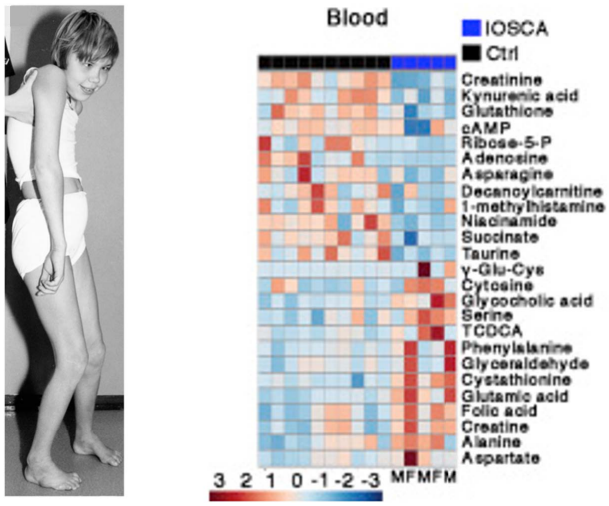


Figure 9: An IOSCA patient and 25 most significantly changed metabolites in IOSCA patient blood. Figure modified from Nikkanen et al. (2016).

A mouse model has been generated for IOSCA and it, like patients, had decreased mtDNA content in liver but unlike patients, not in other tissues. The IOSCA mouse brain recapitulated the human disease phenotype with neurodegeneration affecting especially Purkinje cells and large pyramidal neurons of the CA1 hippocampal region. In addition, IOSCA mouse muscle had low dNTP pools and amino acids and their blood shared disease specific metabolite patterns with patients. The mice, however, did not show motor or sensory defects. (Nikkanen et al., 2016)

## 3.2 Activation of an integrated stress response and remodeling of metabolic pathways

Mitochondria are under control of two separate genomes and must therefore actively communicate with the nucleus to achieve coordinated functions. Communication pathways include those from the nucleus to mitochondria and vice versa. These anterograde and retrograde signals are collectively called mitonuclear communication. In times of stress, depending on the specific signal and its severity, mitonuclear communication can develop into an integrated stress response (ISR). The ISR can originate also from other cellular compartments such as the endoplasmic reticulum, and instead of having a cell autonomous response have effects on the whole organism (Quiros et al., 2016).

The integrated stress response begins with phosphorylation of eukaryotic translation initiation factor 2 $\alpha$ (Dalton et al., 2012). It promotes expression of specific stress response genes like ATF4 (activating transcription factor 4) which in turn induces various stress proteins such as ATF3 (activating transcription factor 3) and TRIB3 (tribbles homologue 3) (Quiros et al., 2016). Activation of the stress response shuts down cytosolic translation and tries to restore normal cellular function.

An integrated mitochondrial stress response (ISRmt), specific to mitochondrial dysfunction and not overlapping with stresses originating from other cellular compartments, has been found to be induced in patients, mice and cell lines with mtDNA maintenance and translation defects (Suomalainen and

Battersby, 2017). Defects in oxidative phosphorylation and mtDNA can send retrograde signals to the nucleus via reactive oxygen species (ROS), decreased ATP levels or $Ca^{2+}$ release from mitochondria due to impaired membrane potential. The ISRmt involves upregulation of genes that have an amino acid response element (AARE) in their regulatory region (Tyynismaa et al., 2010). AAREs are bound by activating transcription factors that have been associated with the unfolded protein response. However, unfolded proteins are rarely found in mammalian mitochondria, and in patients the mitochondrial unfolded protein response is only subtly induced (Suomalainen and Battersby, 2017). Instead, in post-mitotic tissues, the proteins from AARE transcripts regulate lipid and glucose metabolism and the anabolic one-carbon cycle (figure 10) (Nikkanen et al., 2016; Bao et al., 2016).

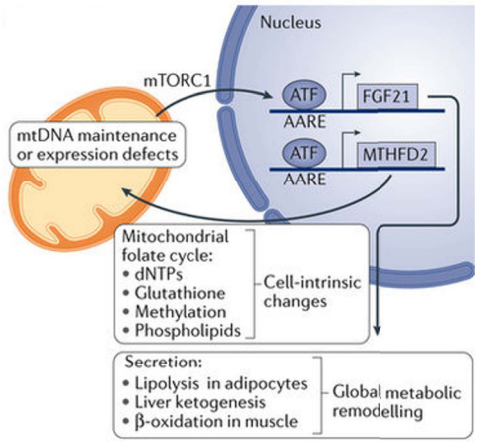


Figure 10: mtDNA expression defects activate an integrated stress response which is driven by activating transcription factors ATF3-5 that recognize amino acid response elements (AARE) in their target genes. ATFs are at least partially controlled by mechanistic target of rapamycin complex 1 (mTORC1). Activation of mitochondrial bifunctional methylene-tetrahydrofolate dehydrogenase 2 (MTHFD2) impacts nucleotide, phospholipid and glutathione synthesis as well as methylation reactions. The ISRmt can also have consequences on systemic metabolism through secreted fibroblast growth factor 21 (FGF21). Figure modified from Suomalainen and Battersby (2017).

One-carbon metabolism is supported by the folate cycle which operates partially inside mitochondria. The folate cycle is regulated by the redox-sensitive enzyme methylene-tetrahydrofolate dehydrogenase 2 (MTHFD2) which has an amino acid response element in its promoter (Tyynismaa et al., 2010). The stress induced folate cycle provides cells with nucleotides, the antioxidant glutathione, NADPH and phospholipids for membrane maintenance. In mitochondrial myopathy, caused by dominant mutations in the mitochondrial helicase Twinkle, MTHFD2 is chronically induced which remodels one-carbon metabolism and causes imbalanced dNTP pools (Nikkanen et al., 2016). Also studies on HEK-cells have shown that mtDNA depletion activates serine biosynthesis and transsulfuration through ATF4 (Bao et al., 2016). However, these pathways have not been well studied in the nervous system.

## 3.3 Impaired redox signaling

All life involves a constant flux of energy which requires complex redox reactions at the cellular level. Redox reactions include all reactions involving the transfer of electrons between chemical substances; oxidation referring to the loss of electrons and reduction to the gain of electrons. Nicotinamide adenine dinucleotide, $NAD^+$ in its oxidized and NADH in its reduced form, and nicotinamide adenine dinucleotide phosphate (NADP), $NADP^+$ when oxidized and NADPH when reduced, are crucial redox agents in all living cells. NADPH is retained mostly in the reduced form to promote reductive anabolic reactions, whereas NAD is mainly maintained in the oxidized form for catabolic reactions (Klingerberg and Buecher, 1960). The separation allows thermodynamically incompatible reactions to occur simultaneously. A correct balance of reducing and oxidizing reactions is crucial for several cellular functions.

The mitochondrial $NAD^+$/NADH ratio is in a more reduced state than the cytosolic one, probably to keep glycolysis occurring in the cytosol and OXPHOS in mitochondria (Cracan et al., 2017). Mitochondrial membranes are not permeable to NADH or NADPH. However, oxidation of NADH in mitochondria results in the same event in the cytosol, at least in cancer cells (Titov et al., 2016). Data from cancer cells shows also that mitochondrial, but not cytosolic, $NAD^+$/NADH and $NADP^+$/NADPH pools are connected (Cracan et al., 2017). Both reduction potentials rely on the activity of major metabolic pathways and shuttle systems. The $NADP^+$/NADPH ratio is mainly determined by the pentose phosphate pathway, one-carbon metabolism, cytosolic malic enzyme and isocitrate dehydrogenase whereas the $NAD^+$/NADH ratio is primarily determined by the TCA cycle, OXPHOS and glycolysis.

The importance of tight regulation of both ratios is an emerging theme as an impaired redox-balance has been connected to diseases like cancer, diabetes and also normal aging (Cracan et al., 2017). The $NAD^+$/NADH ratio signals to multiple pathways. For example in order to keep peroxisomal beta-oxidation ongoing, NADH must be reoxidized to $NAD^+$ and this process might rely on redox-shuttles involving mitochondria (Fransen et al., 2017). Also mitochondrial beta-oxidation requires $NAD^+$ in the step converting 3-hydroxyacyl-CoA to 3-ketoacyl-CoA. Interestingly, both peroxisomal diseases, and those of mitochondrial beta-oxidation, often lead to neurodegeneration with liver involvement (Fransen et al., 2017; Nsiah-Sefaa and McKenzie, 2016).

Reactive oxygen species are highly reactive molecules that can damage major cellular components. ROS are derived from the reduction of oxygen either with a single electron, creating superoxide, two electrons, creating hydrogen peroxide, or three electrons, creating the hydroxyl radical. Respiratory chain complexes I and III are the primary sources of ROS in mitochondria and mitochondria the major sources of ROS in cells (Murphy, 2009; Muller et al., 2004; Turrens, 2003). A dysfunctional respiratory chain is more prone to produce ROS. The primary mitochondrial ROS is superoxide ($O_2^-$) which is converted to hydrogen peroxide ($H_2O_2$) by superoxide dismutases, both in mitochondria and in the cytosol. Hydrogen peroxide can be reduced to water or partially reduced to form the hydroxyl radical (OH), which is one of the strongest oxidants in nature (Turrens, 2003). ROS can damage major components of cells: lipids, nucleic acids and proteins, and alter cellular survival and differentiation (Hamanaka and Chandel, 2010).

The brain, and especially neurons, are vulnerable to oxidative stress because they have a low antioxidant defense capacity, high oxidative metabolism rate and a high concentration of unsaturated fatty

acids which are prone to lipid peroxidation (Belanger et al., 2011). Several neurodegenerative diseases have been associated with oxidative stress. About a tenth of familial amyotrophic lateral sclerosis (ALS) cases have been linked to mutations in the superoxide dismutase coding gene SOD1 (Valentine and Hart, 2003), and a knockdown of SOD2 to cause similar histopathology as seen in Leber hereditary optic neuropathy (Qi et al., 2003). Furthermore, postmortem brain biopsies from Alzheimer's, Parkinson's and ALS patients show ROS damage in affected brain areas (Niedzielska et al., 2016).

# 4 Modeling neurodegeneration on a dish

## 4.1 Induced pluripotent stem cells

Stem cells are undifferentiated cells with unlimited proliferation capacity and ability of giving rise to differentiated cells. Pluripotent cells can give rise to all three germ layers and all cell types except placental cells and cells of the fetal membrane. The three germ layers include the endoderm, ectoderm and mesoderm. Endodermal cells give rise to epithelial cells of the gastrointestinal system, lungs and airways, ectodermal cells to neural cells and skin cells, and mesodermal cells to cells of the connective tissue, muscles and blood. Pluripotent embryonic stem cells (ES cells) can be isolated from an early-stage embryo. Autologous sources of stem cells are bone marrow, adipose tissue and blood. Most adult stem cells are multipotent. Multipotent stem cells are capable of differentiating into more than one cell type but their differentiation capacity is more limited than that of pluripotent stem cells. (Alberts et al., 2002)

A method for reprogramming already differentiated adult skin fibroblasts to pluripotent stem cells was established in 2006 (Takahashi and Yamanaka, 2006). Retroviral transduction of the four transcription factors Oct3/4, Sox2, c-Myc, and Klf4 reverted fibroblasts to a stem cell state where they expressed ES cell markers and morphologically resembled ES cells. Furthermore, the reprogrammed cells were capable of differentiating into all three germ layers after subcutaneous transplantation to nude mice. These genetically engineered pluripotent cells were named induced pluripotent stem cells. iPS cells were expected to revolutionize the field of stem cell therapy but risks of tumorigenesis have not yet been overcome. However, iPS cells are currently valuable tools for disease modeling and drug discovery. Harvesting disease associated tissues or cells is not always possible and collecting stem cells is considered invasive. Instead, patient fibroblasts can be isolated from a simple skin biopsy, genetically engineered to a stem cell state and then differentiated to relevant cell types.

## 4.2 Neuronal differentiation *in vivo* and *in vitro*

During early development, the ectodermal germ layer gives rise to the neuroectoderm, which transforms into the neural plate, neural groove and neural tube, and all mammalian neurons are ultimately derived from neuroepithelial cells of the neural plate and neural tube (Tortora and Derrickson, 2012). The human cortex accounts for three quarters of the brain and is its integrative and executive center. Approximately 80% of cortical neurons are excitatory glutamatergic neurons and the remaining 20% inhibitory GABAer-

gic neurons (Florio and Huttner, 2014). *In vivo*, glutamatergic neurons differentiate from cortical stem and progenitor cells, whereas GABAergic neurons develop outside the cortex and migrate in during development (Wonders and Anderson, 2006). Human cortical neurogenesis spans probably almost a 100 day period (Caviness et al., 1995). In a diseased brain, the cortex is the site of epilepsy and a subject of neurodegeneration. The human neural stem and progenitor population consists of three major groups of cells: apical, subapical and basal progenitors, which are grouped based on the location where they undergo mitosis (figure 11) (Florio and Huttner, 2014).

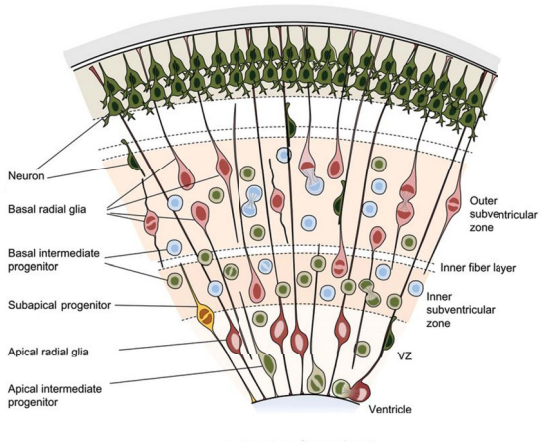


Figure 11: Apical, subapical and basal progenitors are the three main groups of neural progenitors giving rise to all cortical neurons. Neuroepithelial cells dominate the apical region and are therefore not depicted in the figure. Figure adapted from Florio and Huttner (2014).

Neuronal differentiation has been accomplished *in vitro* using several different methods. Neural cells can be generated by reprogramming somatic cells first to stem cells, and then directing their differentiation towards neural cells. Also direct reprogramming, or trans-differentiation, of somatic cells directly to neural cells has been succesfull with different combinations of transcription factors (Ring et al., 2012; Yoo et al., 2011; Vierbuchen et al., 2010). The ultimate goal is to generate functional neuronal networks *in vitro* that resemble disease relevant networks found *in vivo*. Stem cells differentiating *in vitro* undergo similar stages seen *in vivo*. Human pluripotent stem cells, such as iPS cells, resemble the inner cell mass of the early-stage embryo. Differentiation into neuroepithelial cells and rosette-type neural progenitors *in vitro* mirror the formation of the neural plate and neural tube, respectively, *in vivo*. Rosette-type progenitors give rise to radial glial like neural progenitors, and further to neurons and glial cells. (Mertens et al., 2016)

One commonly used method for neuronal differentiation is a suspension culture that does not drive differentiation towards any specific neuronal subtype. In this method, pluripotent cells are collected on a low attachment culture plate and cultured as free floating spheres, neurospheres, for several weeks in a defined culture medium, after which they are plated as small aggregates on a surface that supports their terminal differentiation and maturation. With this method, human embryonic stem cells spontaneously form electrically active neuronal networks (Lappalainen et al., 2010; Heikkila et al., 2009).

Another common method utilizes small molecule inhibitors to direct pluripotent cells towards the neuronal lineage. Neural progenitors have been successfully generated by blocking two signaling pathways that utilize SMADs as transcription factors: TGF-$\beta$ signaling and bone morphogenic protein (BMP) signaling (Chambers et al., 2009). The method is referred to as dual SMAD inhibition. A model for the underlying mechanisms proposes that TGF-$\beta$ inhibition destabilizes TGF/activin- and Nanog-mediated pluripotency and suppresses mesodermal fates, whereas BMP inhibition promotes neuralization of early ectoderms. Dual SMAD inhibition has driven over 80 percent of human ES and iPS cells to express the early neural progenitor marker Pax6 (Paired box 6) in 11 days (Chambers et al., 2009). Furthermore, combining dual SMAD inhibition with retinoid signaling has increased the efficiency of neural induction, as over 95 % of cells have been driven to express neural progenitor markers in 15 days (Shi et al., 2012b).

A high initial cell density favors the generation of cells of the central nervous system, and a low density of cells of the neural crest (Chambers et al., 2009). Both human embryonic and iPS cells form cortical rosettes that are polarized similarly to the cortical neuroepithelium, and give rise to a mixed population of apical and basal progenitors (Shi et al., 2012b). After allowing the progenitors to mature, they start to express glutamatergic but not GABAergic neuronal markers (Shi et al., 2012b). GABAergic neurons can be obtained by ventralizing the progenitors by inhibiting hedgehog signaling (Shi et al., 2012b). Neural progenitors obtained by dual SMAD inhibition can be further differentiated towards the desired neuronal subtype. Terminal differentiation to midbrain dopaminergic and spinal motorneurons (Chambers et al., 2009) as well as electrically active cortical neurons (Shi et al., 2012b) has been succesfull. The proposed model of mechanisms underlying neuronal differentiation by dual SMAD inhibition is presented in figure 12.

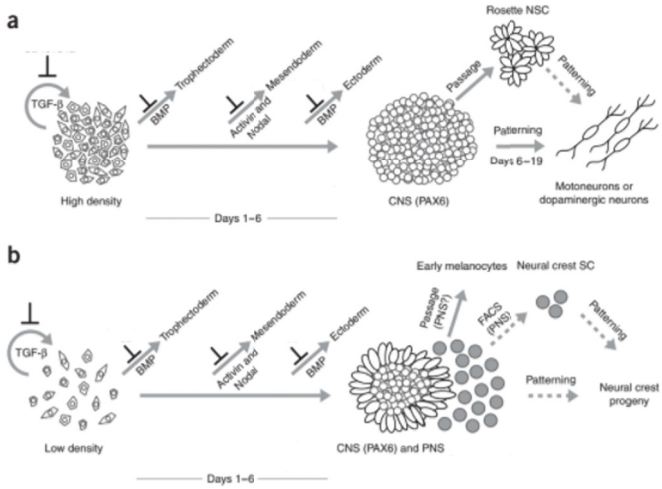


Figure 12: Model of mechanisms underlying neuronal differentiation by dual SMAD inhibition proposed by Chambers et al. (2009). A. A high initial cell density favors the formation of Pax6 positive cells of the central nervous system (CNS), which can give rise to rosette type neural stem cells (NSCs) and patternable neuronal subtypes. B. A low initial cell density gives rise to both cells of the CNS and PNS (peripheral nervous system). Solid arrows indicate demonstrated cell fates whereas dashed arrows indicate proposed fates. Figure modified from Chambers et al. (2009).

## 4.3 Cellular models of neuronal diseases

Diseases of the nervous system are ones of the most difficult to study because taking a biopsy of the manifesting cell types, neuronal cells, is typically not possible. However, many patient-derived iPS cell lines have been successfully created and differentiated to disease relevant neuronal cell types. Successful attempts include neuronal cultures from Alzheimer's disease patients (Israel et al., 2012), motor neurons from ALS patients (Dimos et al., 2008) but also neurons from patients with rarer diseases such as spinocerebellar ataxia type 2 (Xia et al., 2013). Not only has it been possible to obtain the cell types of interest, but they have shown disease related changes such as susceptibility to huntingtin aggregate formation in Huntington's disease patient-derived neurons (Jeon et al., 2012) and accumulation of Lewy bodies in iPS cell-derived dopaminergic neurons of a Parkinson's disease patient (Sanchez-Danes et al., 2012).

Patient-derived iPS cells and therefore also neuronal cells differentiated from them, carry the same genetic variants that cause the disease. Furthermore, the disease causing mutations sit on the exactly same genetic background as they do in patients. Modeling a disease with patient-derived cells has also challenges. The magnitude of differences between iPS cell lines generated from the same individual have not been fully addressed yet. Therefore, it is not known if the seemingly random differences between iPS cell lines can hide those caused by changes due to the disease causing genetic variants. Ideally, each patient cell line would have an isogenic control, meaning the same cell line with the disease causing variant corrected by gene editing, resulting in two cell lines with identical nuclear genomes, except for the presence or absence of the mutation.

# 5 Aims of the study

The aims of this thesis were to:

1. Obtain IOSCA patient-derived neural cells that would manifest a neuronal phenotype related to the disease.

2. Analyze molecular and metabolic consequences of the mutant form of Twinkle, to shed light on the pathogenic cellular and molecular mechanisms underlying symptoms in IOSCA.

# 6 Materials and methods

## 6.1 Culture of iPS cells

IPS cells were cultured on Corning Matrigel Matrix (Sigma-Aldrich) coated wells in Essential 8 medium (Thermo Fisher Scientific) and passaged with 10mM ethylenediaminetetraacetic acid (EDTA).

## 6.2 Neuronal differentiation

### 6.2.1 Differentiation as neurospheres - Method 1

For this work, frozen 4-6 week old neurospheres were rapidly thawed, and transferred on ultra-low attachment well plates (Thermo Fisher Scientific) in neural differentiation medium (NDM) containing 1:1 DMEM/F12:Neurobasal medium supplemented with 2 mM GlutaMAX, 1x B27, 1x N2 and 25 $\mu$g/ml penicillin/streptomycin (All from Gibco Thermo Fisher Scientific), and 20 ng/ml basic fibroblast growth factor (bFGF) (Sigma-Aldrich). The spheres were manually cut twice each week into smaller spheres (maximum diameter 500 $\mu$m) to expose most cells to the medium and avoid differentiation towards unwanted cell lineages. Half of the culture medium was changed three times each week. The spheres were cultured for 3,5 weeks to obtain 7.5-9.5 week old neurospheres. For neuronal differentiation the spheres were manually cut into small aggregates and plated on human laminin (Sigma-Aldrich) coated (10 $\mu$g/ml for polystyrene and 15 $\mu$g/ml for glass coverslips) 12 and 24 well plates in NDM without bFGF. On day 3 after plating, the medium was changed into Neurobasal medium with 1x B27, 1x GlutaMAX, 1x CultureOne supplement (Thermo Fisher Scientific), 0.1 mM ascorbic acid and 0.25x penicillin/streptomycin. The differentiation process is depicted in figure 13.

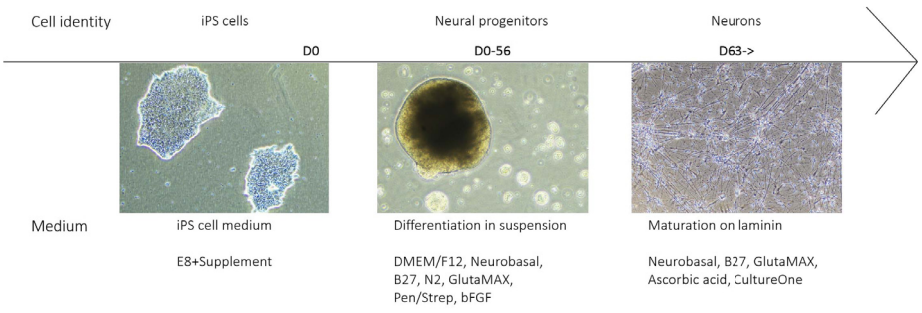


Figure 13: Neural differentiation as neurospheres.

### 6.2.2 Differentiation via dual SMAD inhibition - Method 2

For method 2, iPS cells were cultured until nearly confluent, and then medium was changed to neural induction medium (NIM) containing 1:1 DMEM/F12:Neurobasal medium, 0.5x N2 supplement, 0.5x B27 supplement, 0.5x GlutaMAX, 0.25x penicillin/streptomycin, 0.1 mM ascorbic acid (Santa Cruz), 2 $\mu$M BMP Inhibitor II and 2 $\mu$M TGF-$\beta$ RI kinase inhibitor VI (both from Merck). Cells were cultured in NIM for 7-9 days with a daily medium change. Cells were then detached with 50 mM EDTA and plated on human laminin coated wells in the same medium without dual SMAD inhibition but with 20 ng/ml bFGF, at a cell density of 600 000 cells/cm$^2$. After 2 days bFGF was removed and after 3-5 more days medium changed to terminal differentiation medium containing Neurobasal medium, 1x B27, 1x GlutaMAX, 1x CultureOne supplement, 0.1 mM ascorbic acid and 0.25x penicillin/streptomycin. Differentiation via dual SMAD inhibition is presented in figure 14.

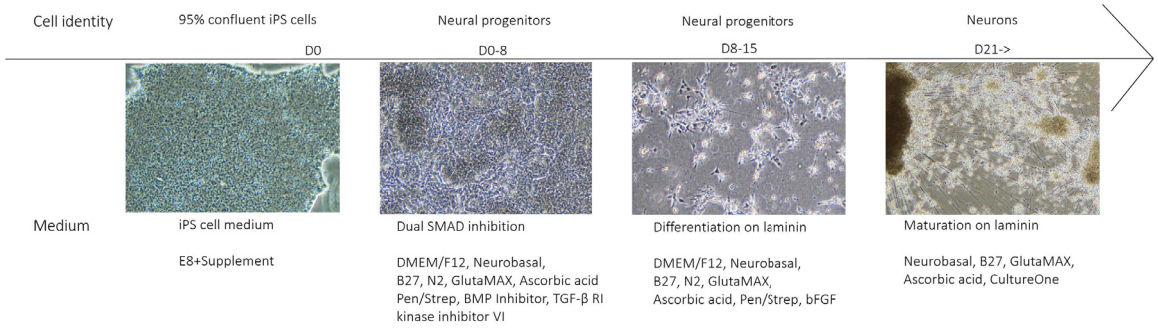


Figure 14: Neural differentiation by dual SMAD inhibition.

## 6.3 Immunocytochemistry

For immunocytochemistry, cells were fixed with 4% paraformaldehyde for 15 minutes in room temperature, or with -20°C acetone for 2 minutes on ice when cells were on glass coverslips. The cells were washed with phosphate-buffered saline (PBS), permeabilized with 0.1% Triton-X100 (Sigma-Aldrich) and blocked using 10% horse serum and 1% bovine serum albumin (BSA) in PBS for 45 minutes in room temperature. Cells were then washed with 1% horse serum, 0.1% Triton-X100 and 1% BSA in PBS and incubated with the primary antibodies in the same buffer overnight in +4°C. After three washes with 1% BSA in PBS, the cells were incubated with the secondary antibodies protected from light for 1 hour in room temperature. The cells were finally washed twice with PBS and twice with PB, dried and mounted with Vectashield containing DAPI (4',6-diamidino-2-phenylindole) (Vector laboratories). All antibodies and working dilutions used in this work are presented in figure 15.

| Target | Antibody number | Dilution | Secondary Antibody 1:400 | Antibody number |
|---|---|---|---|---|
| Nanog | #4893 Cell Signalling Technology | 1:2000 | Goat anti-mouse Alexa 594 | A11005 InVitrogen |
| SSEA4 | MC-813-70 Pierce Thermo Scientific | 1:500 | Goat anti-mouse Alexa 594 | A11005 InVitrogen |
| Lin28A | #3695 Cell Signalling Technology | 1:400 | Chicken anti-rabbit Alexa 488 | A21441 Life Technologies |
| Oct3/4 | sc-9081 Santa Cruz Biotechnology | 1:200 | Chicken anti-rabbit Alexa 488 | A21441 Life Technologies |
| Pax6 | 42-6600 Thermo Fisher Scientific | 1:125 | Chicken anti-rabbit Alexa 594 | A21442 Life Technologies |
| MAP2 | NB300-213 Novus Biologicals | 1:2000 | Goat anti-chicken Alexa 594 | A11042 Life Technologies |
| CI/NDUFB4 | ab110243 Abcam | 1:200 | Donkey anti-mouse Alexa 488 | A21202 InVitrogen |
| CII/SDHA | ab14715 Abcam | 1:2000 | Donkey anti-mouse Alexa 488 | A21202 InVitrogen |
| CIV/MTCO1 | ab14705Abcam | 1:200 | Donkey anti-mouse Alexa 488 | A21202 InVitrogen |
| TOM20 | sc-11415 Santa Cruz Biotechnology | 1:250 | Donkey anti-rabbit Alexa 444 | A21206 Life Technologies |
| MAP2 | NB300-213 Novus Biologicals | 1:1000 | Goat anti-chicken Alexa 680 | ab175779 Abcam |
| TOM20 (F-10) | sc-17764 Santa Cruz Biotechnology | 1:250 | Donkey anti-mouse Alexa 488 | A21202 InVitrogen |
| LC3B | NB600-1384 Novus Biologicals | 1:200 | Chicken anti-rabbit Alexa 594 | A21442 Life Technologies |
| Calreticulin | ab2907 Abcam | 1:1000 | Chicken anti-rabbit Alexa 594 | A21442 Life Technologies |

Figure 15: Antibodies used in this work.

## 6.4 Gene expression analyses

Frozen cell pellets were homogenized and total RNA was extracted by pipetting into TRIzol (InVitrogen). RNA concentration was quantified with Nanodrop and 500 ng of RNA was used to generate cDNA with Maxima first-strand cDNA synthesis kit (Thermo Fisher Scientific). CDNA was amplified with iQ SYBR Green Supermix (Biorad) on CFX96 Touch qPCR system (Biorad). Amplification levels of analyzed genes were normalized to reference housekeeping genes. All primer pairs used in this study are presented in figure 16. Gene expression data is presented as fold change.

| | Target | Forward primer | Reverse primer |
|---|---|---|---|
| Housekeeping genes | Beta-actin | GCCAACCGCGAGAAGATG | CCAGAGGCGTACAGGGATAG |
| | CycloG | TCTTGTCAATGGCCAACAGAG | GCCCATCTAAATGAGGAGTTG |
| Transgenes | Oct4 | AGCGAACCAGTATCGAGAAC | TTACAGAACCACACTCGGAC |
| | Sox2 | AGCTACAGCATGATGCAGGA | GGTCATGGAGTTGTACTGCA |
| | Klf4 | TCTCAAGGCACACCTGCGAA | TAGTGCCTGGTCAGTTCATC |
| | Cmyc | AGCTTTTTTGCCCTGCGTGACC | AGTTTGTGTTTCAACTGTTCTCG |
| Neural precursors | Pax6 | GTGTCCAACGGATGTGTGAG | CTAGCCAGGTTGCGAAGAAC |
| | Nestin | CTAGAGGAGGCAGGTGGTCT | CAAGGTGAAGGGGCATCACT |
| | Musashi-1 | TTCCAAGCCACAACCTACGC | GAATGGCTGTAAGCTCGGGG |
| ISRmt | Atf3 | ATTTTGCTAACCTGACGCCC | CCGTCTTCTCCTTCTTCTTGTTTCG |
| | Atf4 | GTCAGTCCCTCCAACAACAGC | TCCAACGTGGTCAGAAGGTCATC |
| | Atf5 | GCAGGTGATGGCTTCTCTGAC | CCATCTGTTCCAGCTCCTTCTTG |
| | Trib3 | AGCCGCCACCGTATCCCTG | ACAAAGCGACACAGCTTGAGATCAC |
| mtDNA quantification | D-Loop | TGATGTCTGTGTGGAAAGTGG | TTCTTTCATGGGGAAGCAGA |
| | B2M | TGCTGTCTCCATGTTTGATGTATCT | TCTCTGCTCCCCACCTCTAAGT |
| | APP | TGTGTGCTCTCCCAGGTCTA | CAGTTCTGGATGGTCACTGG |
| | cytB | GCCTGCCTGATCCTCCAAAT | AAGGTAGCGGATGATTCAGCC |
| 1C and serine metabolism | MTHFD2 | TGAAGAGCGAGAAGTGCTGA | GAATGCTCCCTGGTGAGGTA |
| | PSAT | AGCAGGAAGGTGTGCTGACT | AAACATCCACTGGCTTGGAC |
| | PHGDH | GGCTCAATGGAGCTGTCTTC | TTCAGTCACATGCTGCTTCC |

Figure 16: Primers used in this work.

## 6.5 mtDNA copy number analysis

DNA was extracted from frozen cell pellets with proteinase K digestion, traditional phenol-chloroform extraction and ethanol precipitation. Relative mtDNA content was analyzed by qPCR using 25 ng of total DNA as a template, similarly as in chapter 6.4. Amplification levels of the mitochondrial gene cytochrome B (cytB) and D-loop were normalized to nuclear genes amyloid-beta protein (APP) or beta-2-microglobulin (B2M), respectively, and are presented as fold change. Primer pairs are presented in figure 16.

## 6.6 Analysis of neuronal morphology and number

Neurons were stained for the neuronal marker MAP2 (microtubule associated protein 2) and all nuclei counterstained with DAPI. Neurons were detected based on their morphology and MAP2 positivity. The percentage of neurons was analyzed from ten randomly taken images of each cell line. The morphology of individual neurons was analyzed from 100 neurons differentiated with M1 and 50 neurons differentiated with M2, for both the disease and control group. Analysis was performed with Simple Neurite Tracer in the Fiji software (https://imagej.nih.gov/ij/; version 1.51n).

## 6.7 Quantification of immunocytochemical stainings

Quantification of fluorescent stainings was done in Fiji software (https://imagej.nih.gov/ij/; version 1.51n) by normalizing the signal intensity of the target to the signal intensity of the neuronal marker MAP2. For all stainings, at least 150 neurons were analyzed for both the disease and control group.

## 6.8 Metabolite extraction and analysis

Samples for metabolomics were extracted from two control cell lines and three IOSCA cell lines differentiated as neurospheres, and two control cell lines and four IOSCA cell lines differentiated with the dual SMAD inhibition method. Four biological replicates were used for each cell line. To extract the metabolites, medium was removed from cells with an aspirator and wells washed twice with 75 mM Ammonium Carbonate in water with pH adjusted to 7.4 with acetic acid. Plates were then snap frozen in liquid nitrogen and stored at -80°C until metabolite extraction in order to reduce sources of variance. Metabolite extraction was performed for all samples with the same reagents on the same day. Metabolites were extracted with two 10 minute incubations with -20°C 40:40:20 acetonitrile:methanol:water solution in -20°C and by scraping the cells after the second incubation. Extracts were centrifuged at 13 000 rpm for 2 minutes in +4°C and supernatants collected for untargeted mass spectrometry.

Untargeted mass spectrometry, as well as annotation and curation of the data, were done in ETH Zurich by Dr. Nicola Zamboni (Williams et al., 2016). Untargeted metabolomics of the iPS cell-derived neural cells captured 503 metabolites. Of the 503 metabolites, metabolites annotated as drugs, toxins and non-mammalian metabolites were removed, after which 388 metabolites remained. The data was obtained as peak intensities for each metabolite, with two technical replicates for each of the four biological replicates. The technical replicates were averaged and the peak intensity table was uploaded to MetaboAnalyst 3.0 (Xia and Wishart, 2016). Before statistical analyses and plotting, peak intensities were normalized by a pooled control sample and log transformed. MetaboAnalyst 3.0 and R were used for analyzing and plotting the data.

## 6.9 Statistical methods

Student's t-test was used for statistical significance analyses. For false positive analyses in metabolomics, p-values were adjusted based on the Benjamini-Hochberg (BH) procedure. P-values of less than 0.05 were considered as significant. All statistical tests were performed with GraphPad Prism 7.03.

# 7 Results and Discussion

## 7.1 Characterization of iPS cells

Three iPS cell lines (C2-C4) and one ES cell line (C1) were used in this study as controls, and four iPS cell lines were derived from patients (I1-I4). All iPS cell lines were first characterized in order to confirm successful reprogramming. All cell lines formed colonies with similar morphology to the embryonic stem cell line and expressed pluripotency markers Nanog, lin28A, Oct3/4 and SSEA4 comparably to the ES cell line (figure 17 and figure 18). Based on the morphology of iPS cell colonies and immunocytochemistry, all iPS cell lines were pluripotent before initiating neuronal differentiation. All control and IOSCA patient-derived iPS cells were analyzed also for their expression of the reprogramming viral transgenes Oct4, Sox2, Klf4 and Cmyc. The reprogramming transgenes were successfully silenced in all iPS cell lines before initiating neuronal differentiation (figure 19).

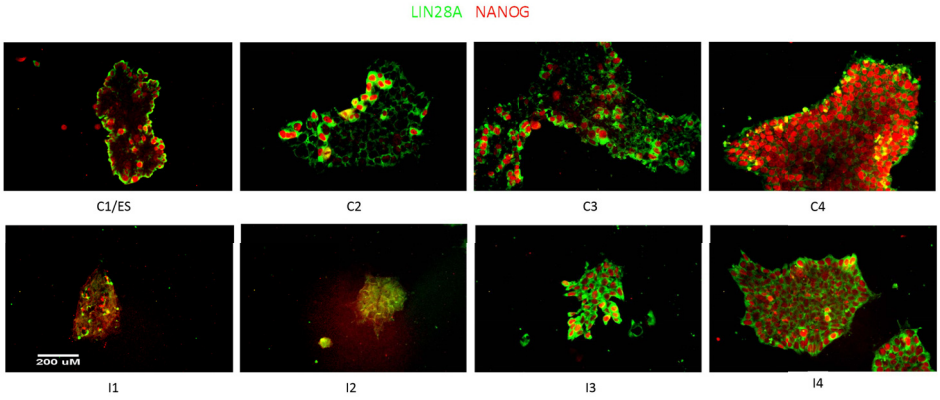


Figure 17: Representative images of the expression of pluripotency markers lin28A and Nanog in control and IOSCA induced pluripotent stem (iPS) cell lines and one control embryonic stem (ES) cell line. All iPS cell lines expressed pluripotency markers and formed colonies with a similar morphology to the ES cell line C1. C1-C4 = control 1-control 4, I1-I4 = IOSCA 1-IOSCA 4.

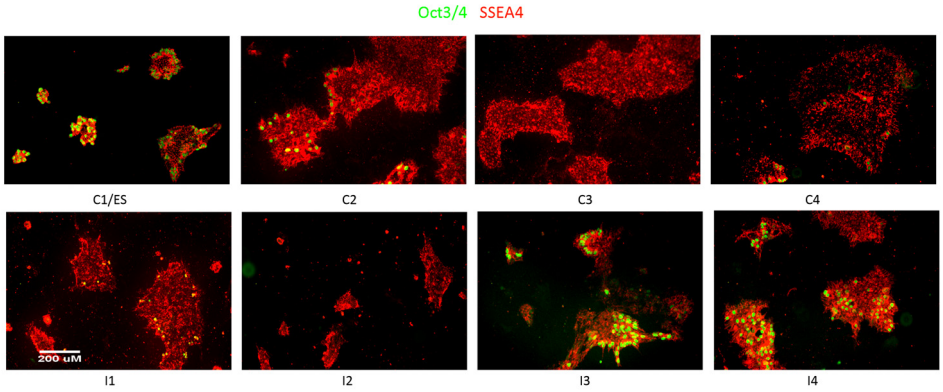


Figure 18: Representative images of the expression of pluripotency markers Oct3/4 and SSEA4 in control and IOSCA iPS cell lines and one control ES cell line.

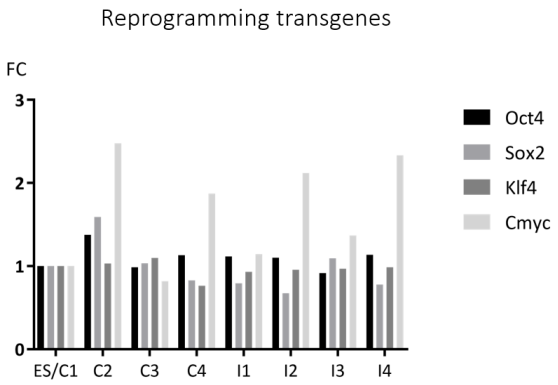


Figure 19: Relative expression of the viral reprogramming transgenes Oct4, Sox2, Klf4 and Cmyc compared to expression in the control ES cell line. Reprogramming transgenes were successfully silenced before neural induction in all used iPS cell lines.

## 7.2 IOSCA patient iPS cells successfully differentiate into neural precursors with M2

Neuronal differentiation was initiated on control and IOSCA patient-derived iPS cells and control ES cells, with the dual SMAD inhibition method, once the cultures were nearly confluent. After eight days in neural induction medium, all cell lines had grown completely confluent and the size of individual cells decreased significantly. Three control cell lines and three IOSCA cell lines were analyzed for their expression of the early neural markers Nestin, Musashi-1 and Pax6 at day eight after neural induction. When compared to expression levels of corresponding iPS cells, all neural precursors expressed Nestin and Musashi-1 with an increase of at least a fold change (figure 20). Pax6 is a transcription factor involved in the development of the brain and spinal cord, and is one of the earliest markers of a transition from pluripotency towards the neural lineage (Zhang et al., 2010). Pax6 showed a substantial upregulation in all cell lines when compared to expression levels in corresponding iPS cells with no differences between control and IOSCA cell lines (figure 20).

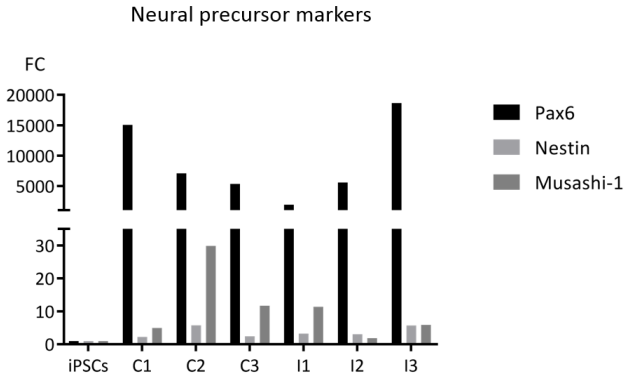


Figure 20: Relative expression of neural precursor markers Pax6, Nestin and Musashi-1 at day eight after initiating neural induction compared to expression in corresponding induced pluripotent stem cells.

Three control cell lines and three IOSCA cell lines were analyzed for their expression of Pax6 at day eight also by immunocytochemistry. Most cells of all analyzed cell lines stained positively for Pax6 and there were no differences between control and IOSCA cell lines (figure 21). After eight days, all analyzed cell lines had successfully transitioned towards the desired neural lineage.

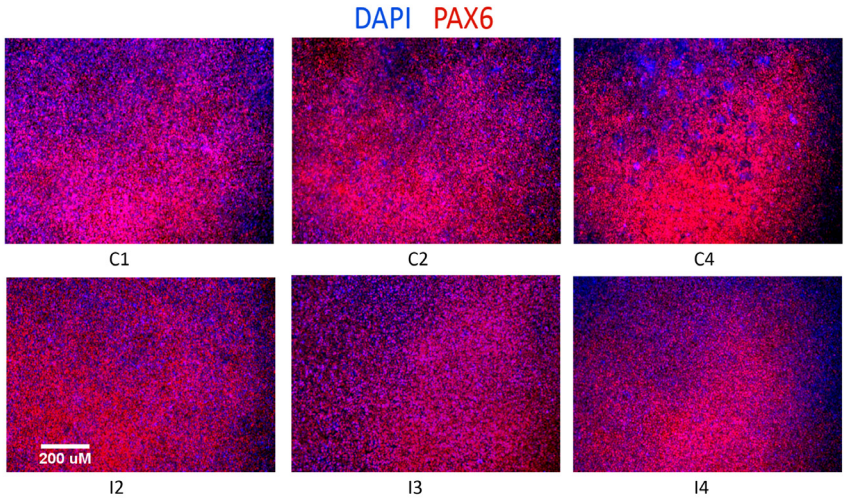


Figure 21: Representative images of the expression of the early neural marker Pax6 eight days after initiating neuronal differentiation analyzed by immunocytochemistry. All analyzed cell lines had successfully transitioned towards the neural lineage at day eight.

## 7.3 Characterization of neural cultures

### 7.3.1 IOSCA neurons show signs of impaired maturation with M1 after two weeks

Neuronal differentiation of iPS cells was performed as described in chapter 6.2.1 on two control cell lines and three IOSCA cell lines, and neurons fixed after two weeks of maturation. The percentage of neurons was significantly lower in IOSCA neural cultures than in controls (figure 22). Contaminating cell types included astrocytes or astrocytic precursors, based on their morphology and modest expression of MAP2, which can be expressed by some astrocytic subtypes, even though being primarily a neuronal marker (Dehmelt and Halpain, 2005). Most contaminating cells, however, were large flat cells without any clear identity and which could be identified easily also under a light microscope. The smaller percentage of neurons in neural cultures obtained from IOSCA cell lines could suggest impaired neuronal differentiation.

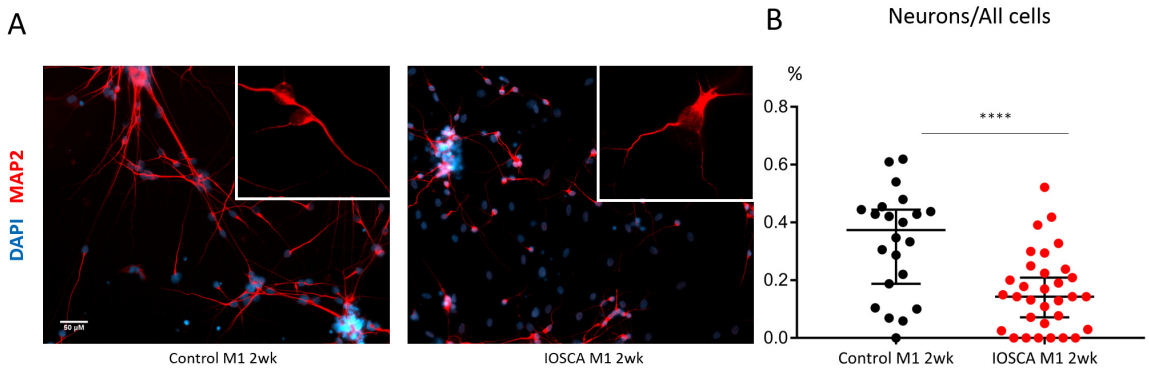


Figure 22: IOSCA patient-derived neural cultures had significantly less neurons than controls, based on their morphology and MAP2 positivity. A. Representative images of control and IOSCA neural cultures after two weeks of maturation. Neurons were stained for the neuronal marker microtubule associated protein 2 (MAP2) and nuclei counter stained with DAPI. B. Quantification of the percentage of neurons from ten randomly taken images per cell line. Error bars indicate standard deviation and data points the percentage of neurons in one image. M1 = differentiation method 1. ****p<0.0001

Also the morphology of individual neurons was analyzed, and interestingly, IOSCA-patient derived neurons were morphologically distinct when compared to controls. While most control neurons were bipolar with far reaching neurites, the patient-derived neurons had a higher number of neurites but they were significantly shorter (figure 22 insets and figure 23). Also the number of branching points in individual neurites was analyzed but no difference was found (figure 23). A reduced percentage of neurons and their distinct morphology could indicate accelerated but impaired neuronal differentiation or maturation in IOSCA. Morphological abnormalities, although different from the results of this work, have been found also in the hippocampal CA1 region of pyramidal neurons in IOSCA mice, as they have been shown to have decreased neurite density, as well as disorganized dendritic trees (Nikkanen et al., 2016).

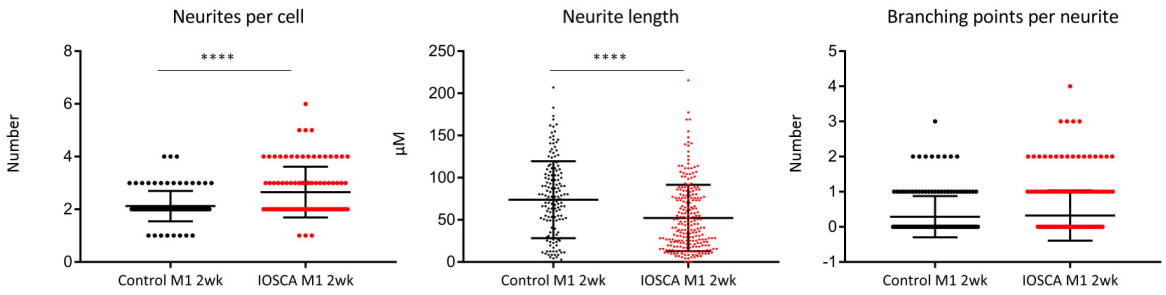


Figure 23: IOSCA patient-derived neurons were significantly more polar but their neurites were shorter than in controls, which could suggest that their differentiation or maturation is impaired. Error bars indicate standard deviation and data points the morphology of individual neurons. ****p<0.0001

### 7.3.2 Neuronal yield is low from cryopreserved neural precursors even after four weeks with M2

Neuronal differentiation of iPS and control ES cells was performed as described in chapter 6.2.2 on four control cell lines and four IOSCA cell lines. Metabolomics-, DNA- and RNA-samples were collected at two weeks after plating neural precursors on laminin-coated wells. Samples that were used for immunocytochemistry were obtained from neural precursors that were cryo-preserved, thawed and plated on laminin-coated glass coverslips to continue with terminal differentiation. However, some cell lines, not depending on their origin, were reluctant to attach and continue proliferation after freezing and thawing. Poly-L-ornithine was added as a second coating material to enhance attachment. Because proliferation and cell growth was extremely slow, cells were kept in culture for four weeks before fixing them for immunocytochemistry. Even at that time point, only two control and two IOSCA cell lines had enough neurons to be analyzed. There were no differences in differentiation capacity between these control and IOSCA cell lines (figure 24). Terminal differentiation of cryopreserved neural precursors yielded a very impure neural culture with a massive amount of contaminating cells. Most of the contaminating cells were ambiguous and distinct of the flat cells and astrocytic precursors obtained from neurospheres.

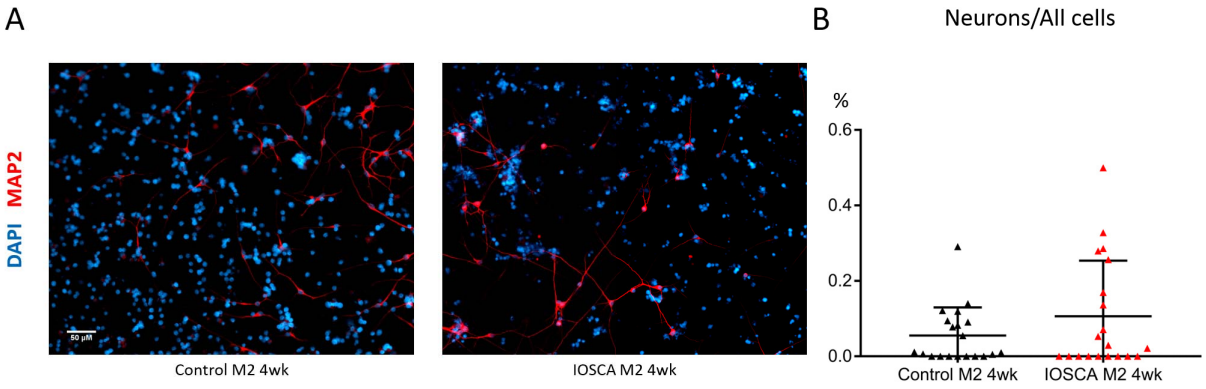


Figure 24: Cryopreserved neural precursors yielded only a low percentage of neurons even at week 4, with no differences between control and IOSCA cell lines when using differentiation method 2. A. Representative images of control and IOSCA patient-derived neural cultures after four weeks of maturation with cryopreserved neural precursors obtained with the dual SMAD inhibition method. Cells were fixed at week 4 due to slow recovery after freezing. Neurons were stained for MAP2 and nuclei counter stained with DAPI. B. Quantification of the percentage of neurons from ten randomly taken images per cell line. Error bars indicate standard deviation and data points the percentage of neurons in one image. M2 = differentiation method 2.

Also for M2, the morphology of individual neurons was analyzed. However, no difference was found in the morphology of control and patient-derived neurons at the analyzed time point of four weeks (figure 25). Unfortunately neuronal morphology was analyzed at two different time points for the two different differentiation methods. It could be that even though the recovery of neuronal precursors differentiated with M2 seemed extremely slow after cryopreservation, the recovered cells had a longer maturation time,

and therefore the controls had enough time to reach the same maturation stage as IOSCA neurons. Therefore, it could be that IOSCA neurons mature faster than wild type neurons *in vitro*, which is seen at two weeks. Furthermore, impaired neuronal differentiation or maturation could be related to the pathology of IOSCA. However, a major differentiation defect would be likely to cause developmental and structural brain defects in patients, which has not been found. In addition, being seen only with one of the differentiation methods, the analysis should be repeated by analyzing different time points using only one differentiation method.

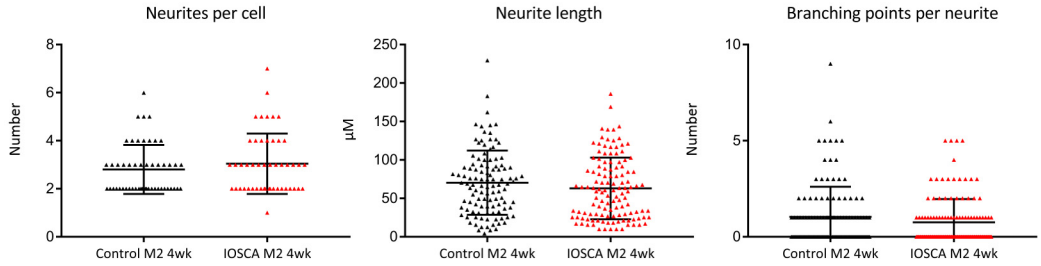


Figure 25: Morphology of individual control and IOSCA patient-derived neurons from cryopreserved neural precursors was similar at the analyzed time point of four weeks, when using M2. Error bars indicate standard deviation and data points the morphology of individual neurons.

## 7.4 IOSCA neural cells do not develop mtDNA depletion in two weeks

Mitochondrial DNA copy number has been shown to be decreased in IOSCA patient brain and liver (Hakonen et al., 2008), and therefore relative mtDNA content was analyzed from the patient-derived neural cells. Because of limited sample size, it was possible to be analyzed only from neural cells obtained with the dual SMAD inhibition differentiation method. However, mtDNA depletion was not significant at two weeks (figure 26). This could be due to a too short culture time for detectable mtDNA depletion to develop, or a masking effect of contaminating cell types, which comprised more than half of the cell population.

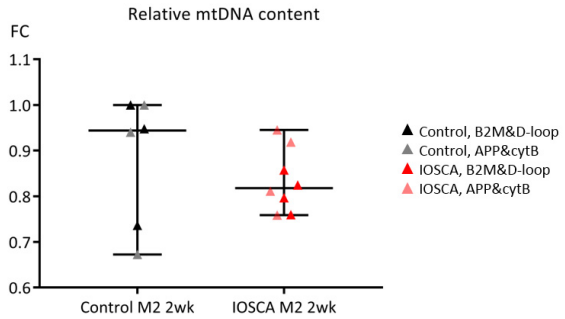


Figure 26: Relative mtDNA content was not significantly altered in IOSCA patient-derived neural cells after two weeks of maturation, when compared to controls. Relative mtDNA content was analyzed by two different primer pairs: B2M and mitochondrial D-loop, as well as APP and mitochondrial cytB. Data is presented as median and error bars indicate interquartile range.

## 7.5 Mitochondrial network is reduced in IOSCA neurons

Because complex I and to a lesser extent also complex IV have been shown to be decreased in IOSCA patient brain (Hakonen et al., 2008), they were analyzed by immunocytochemistry in control and patient-derived neurons. Also CII was analyzed as it is the only one of the respiratory chain complexes that is entirely nuclear encoded. Similarly to patients, CI and CIV were significantly decreased but CII was unaltered in IOSCA patient-derived neurons (figure 27).

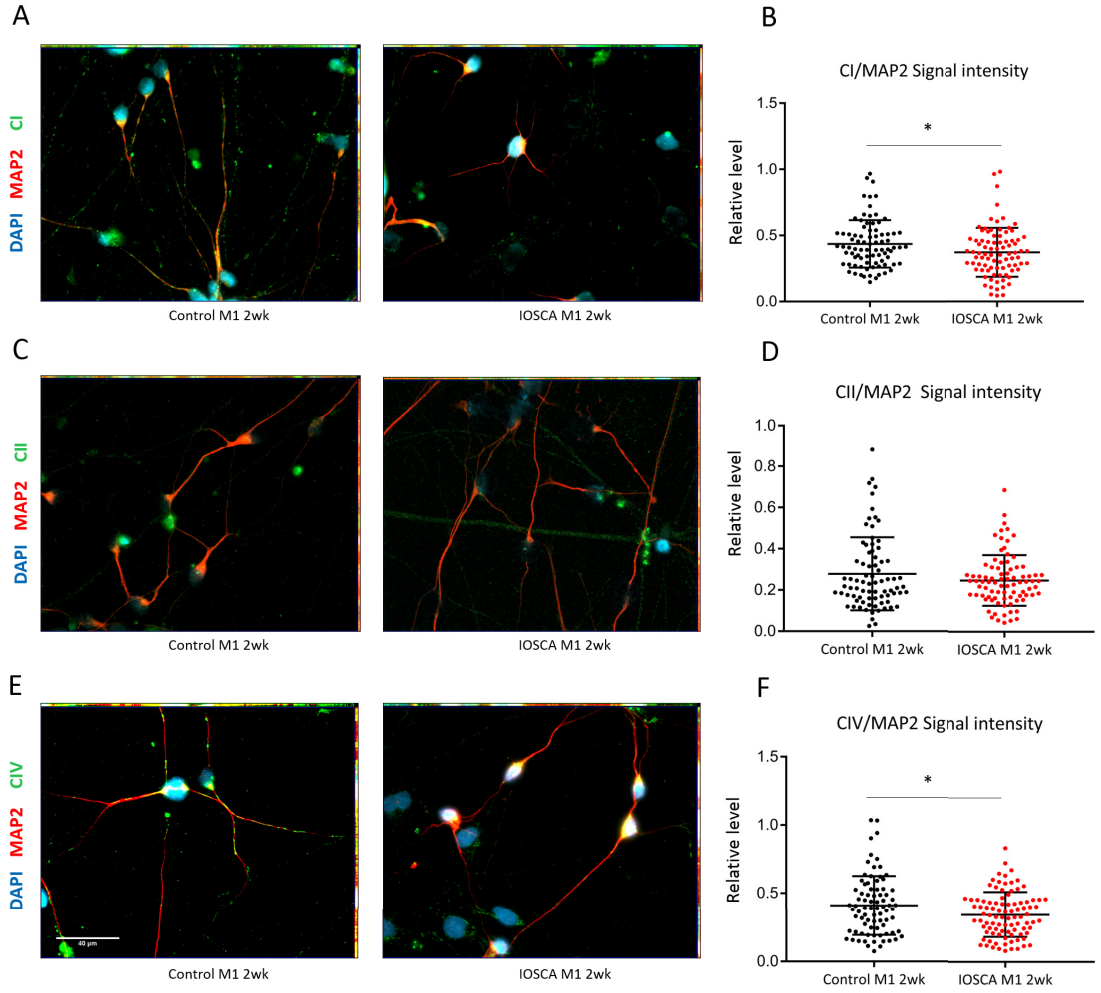


Figure 27: Respiratory chain complexes I and IV were decreased but complex II was unchanged in IOSCA patient-derived neurons when compared to controls. A. Representative images of MAP2- and CI-staining in control and IOSCA patient-derived neurons differentiated with M1. B. Quantification of CI/MAP2 signal intensity in control and patient-derived neurons. C. Representative images of MAP2- and CII-staining in control and patient-derived neurons. D. Quantification of CII/MAP2 signal intensity in control and patient-derived neurons. E. Representative images of MAP2- and CIV-staining in control and patient-derived neurons. F. Quantification of CIV/MAP2 signal intensity in control and patient-derived neurons. Data points represent RC complex signal intensity/MAP2 signal intensity in individual neurons. Error bars indicate standard deviation. *$p<0.05$

Also the total mitochondrial network was visualized and analyzed by staining for mitochondrial import receptor subunit TOM20 (translocase of outer membrane 20). Surprisingly, IOSCA neurons had significantly less mitochondria, when compared to controls, in neurons differentiated with both methods (figure 28). Patient-derived neurons seemed to have normal mitochondrial networks in the soma but many of their neurites were almost completely empty of mitochondria. CII being unaltered could be explained by a compensatory effect, if patient-derived neurons had induced nuclear-encoded CII, which is a common finding in respiratory chain deficiencies (Hamalainen et al., 2013). However, CII staining was relatively faint in both control and patient neurons and, therefore, this aspect of the experimentation requires further replication.

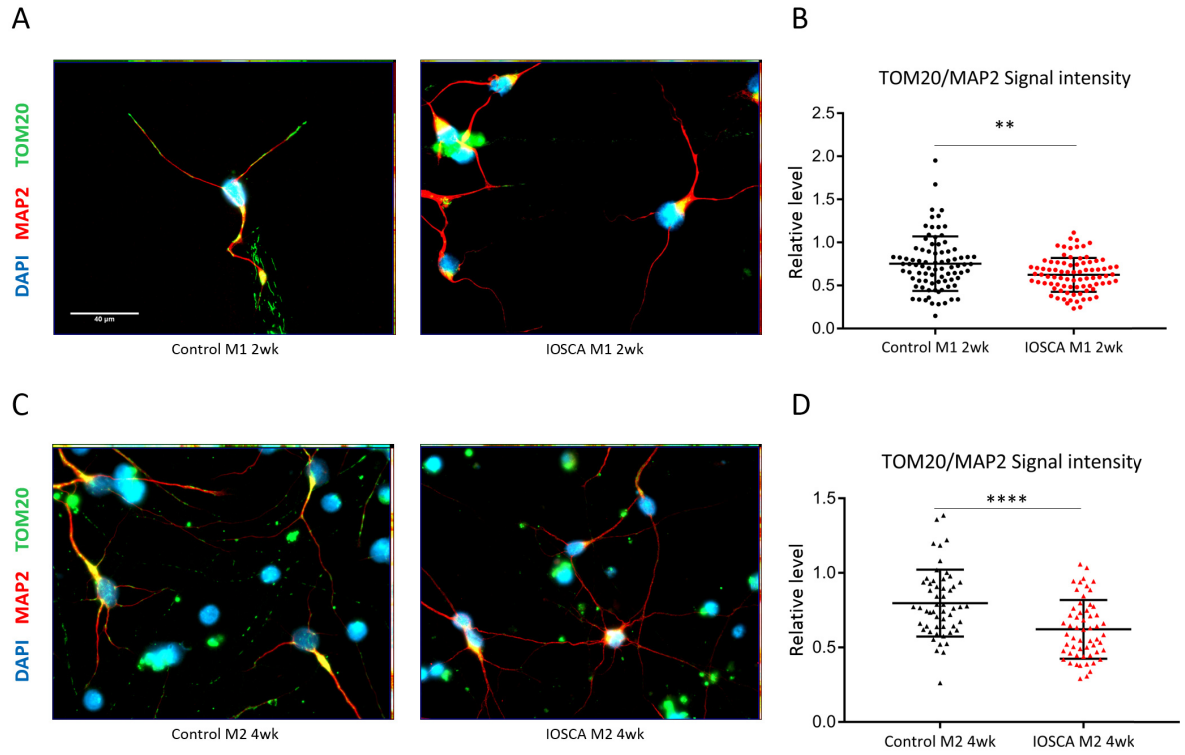


Figure 28: IOSCA-patient derived neurons had reduced mitochondrial networks especially in their neurites, regardless of the differentiation method. A. Representative images of control and IOSCA-patient derived neurons, differentiated with M1, stained for MAP2 and mitochondria stained for translocase of outer membrane 20 (TOM20) after two weeks of maturation. B. Quantification of TOM20/MAP2 signal intensity in neurons differentiated with M1. Data points represent individual neurons. C. Representative images of MAP2 and TOM20-staining in neurons differentiated with M2, with a maturation time of four weeks after cryopreservation. D. Quantification of TOM20/MAP2 signal intensity in neurons differentiated with M2. Data points represent individual neurons. Error bars indicate standard deviation. **p<0.01, ****p<0.0001

To investigate whether the loss of mitochondria was due to excessive mitophagy, autophagosomes were stained for autophagosome membrane marker LC3B and mitochondria for TOM20. Neurons were identified based on their morphology. Immunocytochemistry did not show more colocalization of LC3B and TOM20 in IOSCA patient-derived neurons than in controls. However, if mitophagy occurs mainly around the soma, before mitochondria reach neurites, it would be difficult to detect the event with this method. Therefore, it would be interesting to analyze turnover of mitochondria in live cells, utilizing for example mito-QC (McWilliams et al., 2016).

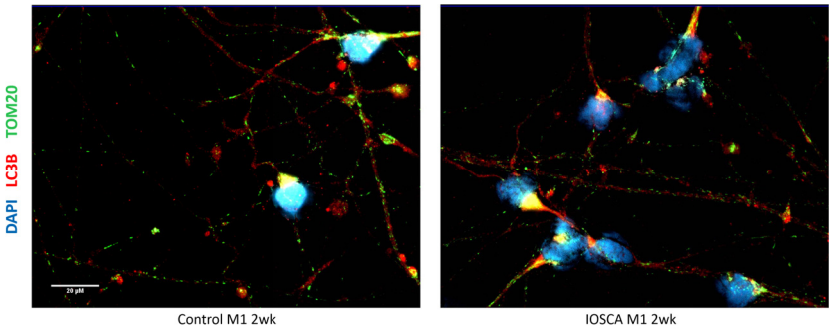


Figure 29: Colocalization of TOM20 with LC3 autophagosome membrane marker was not increased in IOSCA patient-derived neurons.

## 7.6 The ISRmt, one-carbon metabolism and serine biosynthesis are not activated in IOSCA neural cells

The mitochondrial integrated stress response has been shown to be activated in patients and disease models with mtDNA maintenance and translation defects, especially in the heart and muscle (Suomalainen and Battersby, 2017). Therefore, expression of its activating transcription factors 3-5 and TRIB3, were analyzed. None of them, however, were significantly upregulated in patient-derived neural cells when compared to controls (figure 30). The integrated stress response might be tissue or mutation-specific and therefore not relevant for neural cells carrying the IOSCA mutation.

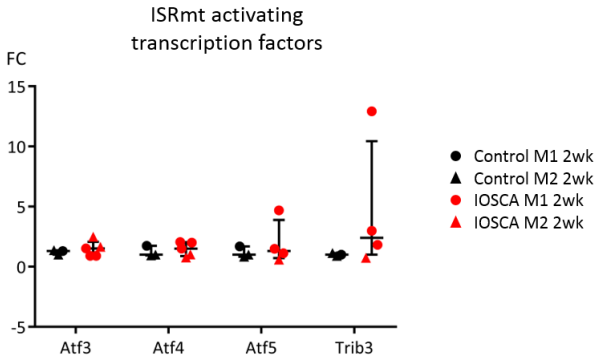


Figure 30: Activating transcription factors 3-5 and TRIB3 of the mitochondrial integrated stress response were not upregulated in IOSCA patient-derived neural cells when compared to controls. Data presented as median and error bars indicate interquartile range.

Dominant mutations of Twinkle, causing mitochondrial myopathy and modeled by the deletor mouse, cause a transcriptional starvation response in muscle (Tyynismaa et al., 2010). This includes the induction of one-carbon metabolism and serine biosynthesis, serine being the primary 1C donor to the mitochondrial folate cycle (Nikkanen et al., 2016). Therefore the expression of one of the key enzymes of the 1C cycle, MTHFD2, and two of serine biosynthesis, PHGDH and PSAT1, were analyzed by qPCR. However, no significant changes were seen in the expression of any of the analyzed enzymes (figure 31). The strong induction of serine biosynthesis and one-carbon metabolism in deletor muscle could be tissue or mutation specific and, therefore not relevant to IOSCA neural cells.

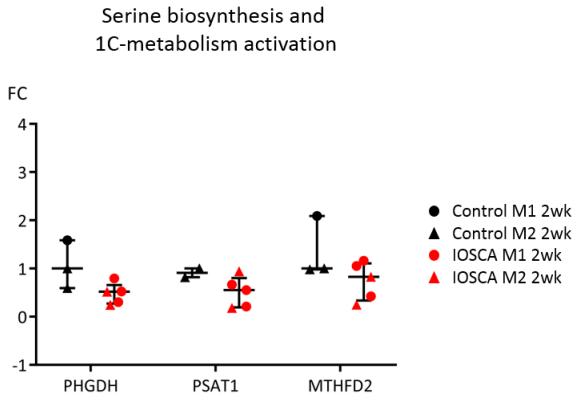


Figure 31: Expression of MTHFD2, a key enzyme in the mitochondrial folate cycle, and PSAT1 and PHGDG, key enzymes in serine biosynthesis, were not upregulated in IOSCA patient-derived neural cells. Data presented as median and error bars indicate interquartile range.

## 7.7 Major metabolic pathways are altered in IOSCA neural cells

Metabolic profiling of control and IOSCA neural cells was performed by untargeted mass spectrometry. Untargeted metabolomics revealed genotype-specific metabolic profiles, independent of the used neuronal differentiation method as seen in figure 32 A. Metabolites most contributing to the variance between IOSCA and control groups are presented in figure 32 B. The metabolite contributing most to the variance of the two groups was N-acetyl-L-aspartic acid (NAA, Acetyl-Asp), which was lower in IOSCA patient-derived neural cells when compared to controls. NAA is one of the most abundant metabolites in the brain, and synthesized in neurons from aspartate and acetyl-CoA. It is a precursor for the neurotransmitter N-acetylaspartylglutamic acid and it plays a role in energy metabolism in neuronal mitochondria. The reason for NAA being the top hit could be simply because IOSCA neural cultures had a smaller percentage of neurons. However, decreased NAA could also reflect neuronal and especially axonal damage.

IOSCA neural cells had an increased amount of two ceramides, C16-ceramide and C18-ceramide, which both are strong signals for apoptosis. Ceramides can be produced by hydrolysis of sphingomyelin or by de novo synthesis from serine and palmitate. Sphingomyelin is a key plasma membrane component which can be hydrolysed by either neutral or acidic sphingomyelinase, of which the neutral sphingomyeli-

nase is sensitive to oxidative stress. Abnormal sphingolipid metabolism has been seen in ALS patients and mice, whose motor neurons were hypothesized to degenerate due to oxidative stress induced accumulation of long-chain ceramides and cholesterol esters (Cutler et al., 2002). Notable is also that glutathione, the end product of the transsulfuration pathway, was low in IOSCA neurons, as was AMP, an intermediate in purine synthesis, and a precursor of ATP. Low glutathione and disturbed purine synthesis have been found also in patient blood (Nikkanen et al., 2016). Glutathione is an important antioxidant in the brain and therefore, the amount of reactive oxygen species in patient-derived neural cells would be interesting to analyze. Finally, the TCA cycle intermediate isocitrate was low, suggesting a disturbed TCA cycle in patient-derived neural cells.

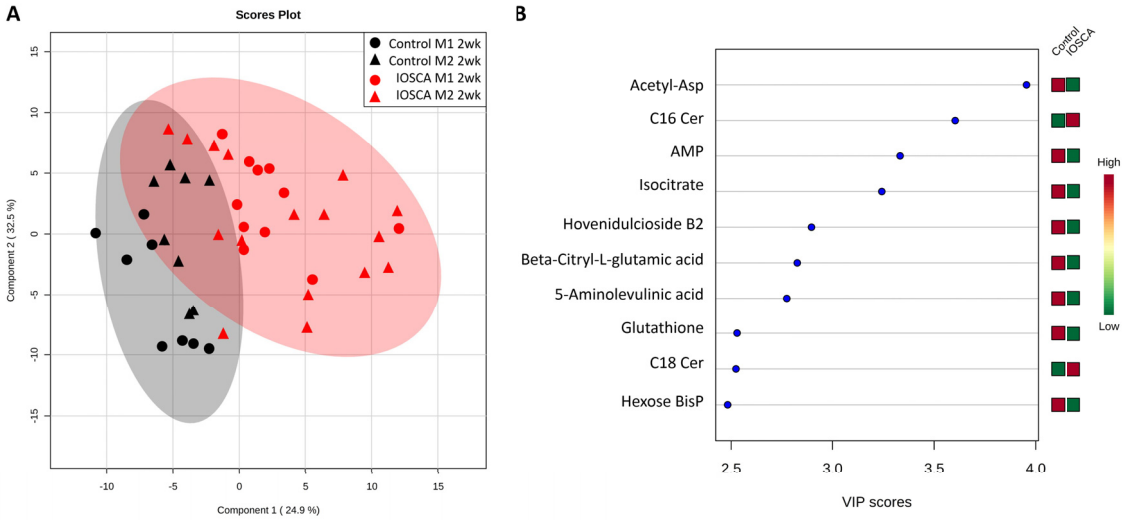


Figure 32: A. Partial least squares discriminant analysis (PLS-DA) showed genotype-specific clustering of control and IOSCA groups, independent of the neuronal differentiation method. B. Highest ranked metabolites based on variable importance in projection (VIP score) for the PLS-DA. Acetyl-Asp = N-acetyl-L-aspartic acid, Cer = ceramide, AMP = adenosine monophosphate, BisP = bisphosphate.

To get an overview of the data, most significantly changed metabolites were visualized on a volcano plot, which is presented in figure 33. Three purine synthesis intermediates, deoxyadenosine diphosphate (dADP), inosine and uridine monophosphate (UMP) were among most significantly decreased metabolites, again highlighting impaired purine synthesis. Most significantly increased metabolites were decenedioic acid and sebacic acid, which have been found in high concentrations in the urine of patients with medium-chain acyl-CoA dehydrogenase (MCAD) deficiency (Tserng et al., 1990). Medium-chain acyl-CoA dehydrogenase is the enzyme involved in the first step of oxidation of medium-chain fatty acids. MCAD deficiency manifests in infancy as hypoglycemia, vomiting, hepatopathy, encephalopathy, seizures and coma (Touma and Charpentier, 1992), symptoms of which hepatopathy, encephalopathy and seizures are shared with IOSCA. Therefore, there is a possibility of some common underlying disease mechanisms.

There has been evidence of a FAO complex having a physical contact with ETC supercomplexes (Wang et al., 2010), and loss of MCAD has been shown to reduce the levels of respiratory chain complexes I, III and IV, as well as the OXPHOS supercomplex, and increase oxidative stress (Lim et al., 2018). Therefore, it would be interesting if similarly an unstable electron transport chain could destabilize FAO enzymes, and lead to the accumulation of medium- and long-chain fatty acids. However, neural mitochondria use fatty acids as fuel only during early development after which they shift to glucose (Erecinska et al., 2004). It is generally accepted that brain tissue has a poor capacity for fatty acid oxidation due to low enzyme activity and slow translocation of long-chain fatty-acid CoA esters across the inner mitochondrial membrane (Yang et al., 1987).

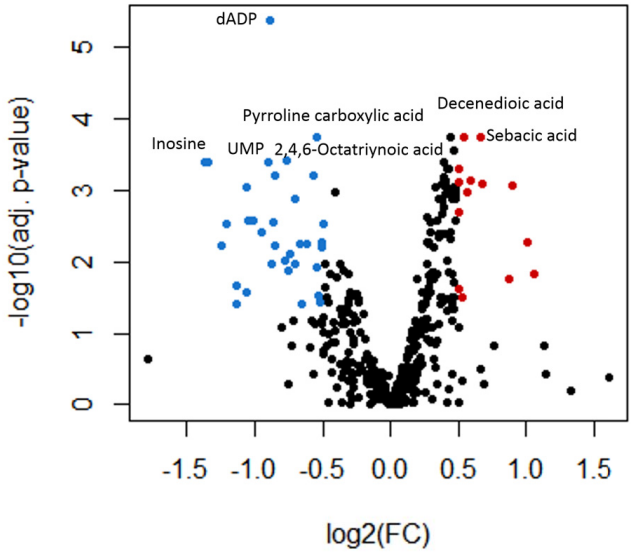


Figure 33: Most decreased metabolites in IOSCA patient-derived neural cells included nucleotide synthesis intermediates deoxyadenosine diphosphate (dADP), inosine and uridine monophosphate (UMP). Two most significantly increased metabolites were medium-chain fatty acids decenedioic acid and sebacic acid. Blue dots indicate decreased and red dots increased metabolites with BH adjusted p-value$<0.05$ and absolute log2(FC)$>0.5$, labeled dots have BH adjusted p-value$<0.001$.

Thirty most altered metabolites in IOSCA patient-derived neural cells were visualized on a heatmap which is presented in figure 34. The heatmap was generated using euclidean distance as distance measure and Ward's method as the clustering algorithm. Neural cells derived from patients and controls showed genotype specific metabolic fingerprints. Nucleotide, especially purine synthesis, intermediates formed a prominent group of decreased metabolites, whereas most metabolites with increased concentration in the patient-derived neural cells were medium- and long-chain fatty acids.

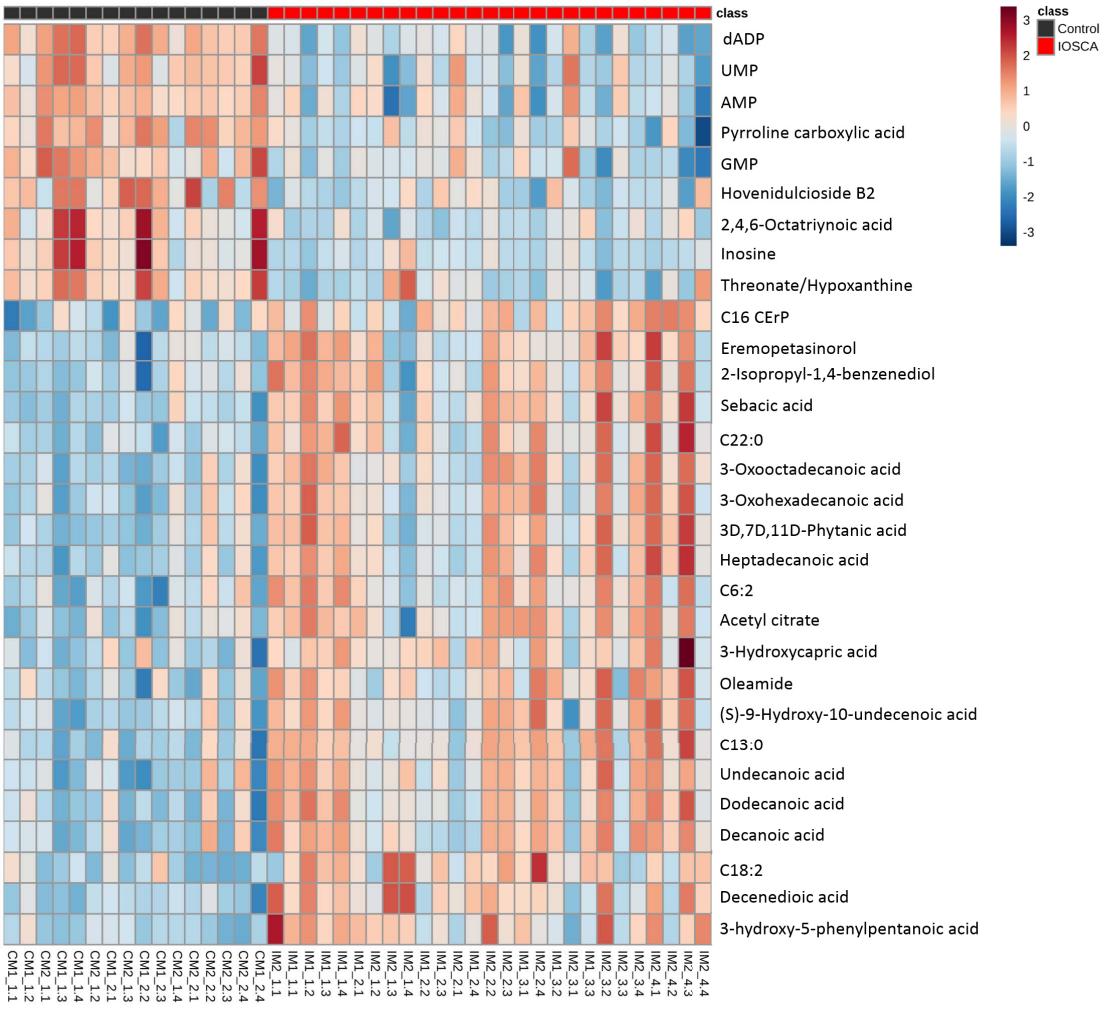


Figure 34: Thirty most significantly increased and decreased metabolites in IOSCA patient-derived neural cells when compared to controls. Purine synthesis intermediates formed a prominent group of decreased metabolites whereas most metabolites with increased concentration were fatty acids. Columns represent individual samples. The heatmap was generated using euclidean distance as distance measure and Ward's method as the clustering algorithm.

Reduced nucleotide synthesis intermediates included dADP, UMP, AMP, GMP, inosine and hypoxanthine. Twinkle has been proposed to hydrolyze dNTPs independent of mtDNA replication, and dNTP pools have been shown to be depleted in IOSCA mouse muscle (Nikkanen et al., 2016). Continuous hydrolysis of dNTPs by mutated Twinkle generates dNDPs and inorganic phosphate which is itself a signaling molecule. Nucleotide synthesis could be increased in IOSCA neurons, in order to replenish dNTP pools, which could exhaust the cells from nucleotide synthesis intermediates. Of one-carbon metabolism, also the end product of the transsulfuration pathway, glutathione, was reduced. Changes in one-carbon metabolism are summarized in figure 35.

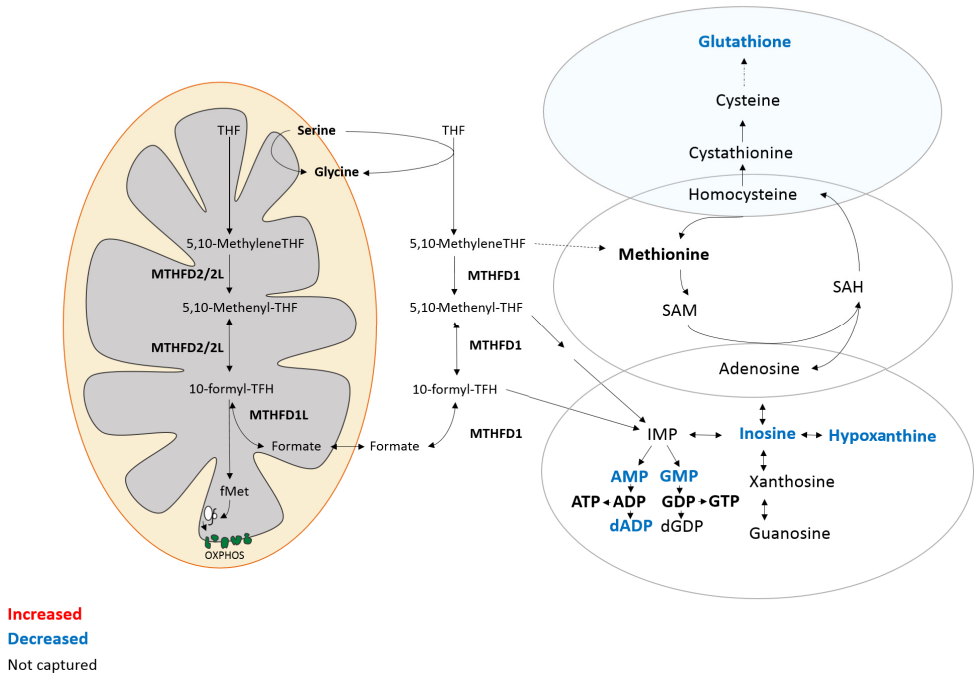


Figure 35: Graphical overview of changes in one-carbon metabolism in IOSCA patient-derived neural cells. Several intermediates of purine synthesis, as well as glutathione, the end product of the transsulfuration pathway, were decreased in IOSCA patient-derived neural cells. P-values adjusted for multiple testing of less than 0.05 were considered significant.

Both de novo and salvage pathway of nucleotide synthesis require 5-phosphoribosyl-$\alpha$-1-pyrophosphate (PRPP), which is also the rate-limiting substrate for both pathways (Becker and Kim, 1987). Also the precursor of PRPP, ribose-5-phosphate, which is produced in the pentose phosphate pathway, can limit nucleotide synthesis (Pilz et al., 1984). The rate limiting enzyme in the oxidative branch of pentose phosphate pathway is mainly regulated by the $NADP^+$/NADPH ratio. There is increasing evidence of the fundamental role of NAD and NADP as regulators of energy metabolism, mitochondrial function, calcium homeostasis and redox metabolism (Ying, 2008). Their balance and ratio with corresponding reduced forms would therefore be critical to be analyzed also in IOSCA neural cells.

Several of the increased metabolites in IOSCA patient-derived neural cells were intermediates of fatty acid synthesis, such as 3-oxodecanoic acid and 3-oxohexadecanoic acid (figure 34). Fatty acids are synthesized from acetyl-CoA and NADPH on a dimeric fatty acid synthase in the cytosol via the successive addition of two carbons on the initial acetyl moiety. The end product is a 16-carbon palmitic acid which can be further modified or elongated. Fatty acids are mainly synthesized in liver, adipose tissue and lactating mammary glands in humans under normal conditions. However, neurons have been shown to activate fatty acid synthesis from glutamine and glutamate under hypoxia (Brose et al., 2014). One regulator of fatty acid metabolism is modulation of acetyl-CoA carboxylase activity. It is

allosterically activated by citrate and glutamate, and reversibly inactivated through phosphorylation by AMPK (Munday, 2002; Boone et al., 2000; Vagelos et al., 1963). The hypoxic neurons were hypothesized to induce fatty acid synthesis through acetyl-CoA carboxylase activity via stimulation of phosphatase by glutamate, and fatty acid synthesis to be an alternative mechanism to utilize hydrogen and end products of glycolysis, while minimizing apoptotic effects of lactate accumulation.

Three TCA cycle intermediates, (iso)citrate, malate and fumarate were decreased suggesting also the TCA cycle to be affected in IOSCA patient-derived neural cells. Noteworthy is that the unstable intermediate oxalosuccinic acid was slightly induced (FC 1.38). Also glutamine, which can be metabolized to $\alpha$-ketoglutarate and fed into the TCA cycle, was decreased. Increased glutaminolysis would provide the cells with NADPH for lipid and nucleotide synthesis. However, lactate was found in similar levels compared to controls, revealing that glycolysis was not induced in IOSCA patient-derived neural cells. Analogously, lactate has not been found to be elevated in homozygous IOSCA patients' cerebrospinal fluid (Koskinen et al., 1994).

The accumulation of long- and medium-chain fatty acids and the decrease in TCA cycle intermediates suggested that the patient-derived neural cells had either channeled their metabolism towards fatty acid synthesis or their inability to utilize already synthesized fatty acids. Therefore, it would be interesting to analyze metabolic flux. Because IOSCA patient-derived neurons had shorter neurites than controls, it could also be that the accumulation of fatty acids was partly due to reduced neurite outgrowth without changes in fatty acid synthesis. Changes in the TCA cycle and fatty acid metabolism are summarized in figure 36. Despite all the changes in major metabolic pathways, ATP was well within control range (figure 37), highlighting that the lack of energy is not key in all mitochondrial diseases.

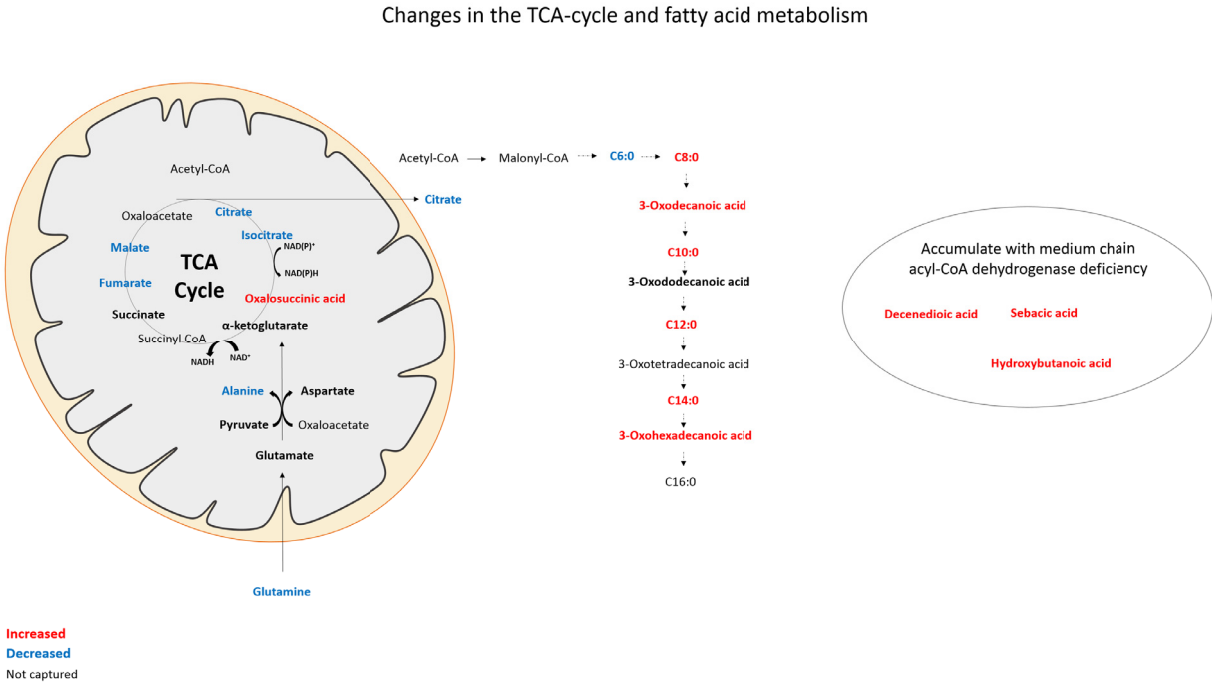


Figure 36: Graphical overview of changes in energy metabolism in IOSCA patient-derived neural cells. Several intermediates of the citric acid cycle were decreased, whereas many intermediates of fatty acid synthesis were increased, in IOSCA patient-derived neural cells. However, there were also signs of impaired fatty acid oxidation as the patient-derived neural cells showed accumulation of some medium-chain fatty acids that have been associated with medium-chain acyl-CoA dehydrogenase deficiency. P-values adjusted for multiple testing of less than 0.05 were considered significant.

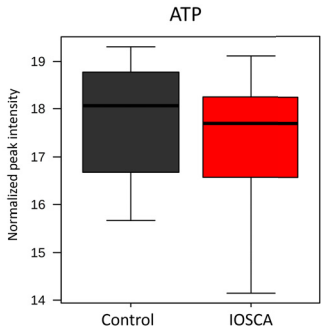


Figure 37: Even though major pathways related to energy metabolism were altered in IOSCA neural cells, ATP levels were comparable to control cells. Data presented as median and interquartile range with normalized values.

Finally, one hallmark of peroxisomal diseases is the accumulation of phytanic acid, which had accumulated also in IOSCA patient-derived neural cells (figure 34). Peroxisomes and mitochondria function together in fatty acid oxidation and bile acid synthesis, and peroxisomal diseases manifest in similar ways as mitochondrial diseases (Fransen et al., 2017). Phytanic acid has been shown to inhibit mitochondrial

respiratory chain complexes I-III as well as synaptic $Na^+/K^+$ ATPase in rat cerebellum, and inhibition of the pump has been associated with excitotoxicity and epilepsy (Busanello et al., 2013), which is one of the symptoms in IOSCA. Therefore, it would be interesting to investigate if the function of peroxisomes is affected in IOSCA neurons.

# 8 Conclusions

Mitochondrial DNA depletion syndromes, such as IOSCA, are often severely disabling diseases that in the worst case lead to early death. Currently therapy is targeted to relieving symptoms and no curative treatments are available. The aim of this thesis was to increase understanding of the molecular consequences of impaired mitochondrial DNA replication specifically in neurons. Even though IOSCA patient-derived neural cells did not develop significant mitochondrial DNA depletion in two weeks, the cells showed structural, organellar and metabolic abnormalities, demonstrating the power of cellular models. Findings of this work may be relevant also for other hepatocerebral mtDNA depletion disorders.

Neurons were obtained with both differentiation methods used in this work. However, the integrity of neuronal differentiation and maturation remains an open question due to inconsistent results with the two different differentiation methods. It would be interesting to analyze the percentage of neurons and their morphology at different time points separately with both methods. A clearly reduced mitochondrial network was replicated in neurons differentiated with both methods. Either mitochondria are unable to pass a check point when leaving the soma, or they are excessively degraded by mitophagy in patient-derived neurons. Mitophagy could be further analyzed using mito-QC (McWilliams et al., 2016) to illuminate mitochondrial turnover in live cells.

Even though the mitochondrial integrated stress response has been shown to be activated in mtDNA maintenance and translation defects, it was not induced in IOSCA patient-derived neural cells. Also one-carbon metabolism and serine biosynthesis, which are induced in dominant mutations of Twinkle, were not activated in IOSCA patient-derived neural cells. Mitochondrial diseases are highly tissue specific and therefore it is not surprising that different signaling and metabolic pathways are vital for different cell types.

Untargeted metabolomics revealed remodeling of major metabolic pathways in IOSCA patient-derived neural cells. At the core of infantile-onset spinocerebellar ataxia is the mutated Twinkle helicase, crucial for faithful replication of mitochondrial DNA. The drained purine synthesis intermediates could be a cause of insatiable nucleotide synthesis. Therefore, it would be interesting to see if nucleotide supplementation would shift the metabolism of patient-derived neurons towards that of control cells. DNMPs have been already successfully used as therapy for a muscle specific mitochondrial DNA depletion disease caused by mutations in TK2 (Garone et al., 2014).

Accumulation of medium- and long-chain fatty acids and impairment of the TCA cycle have not been previously associated with IOSCA, and were therefore somewhat unexpected. The patient-derived neural cells showed signs of both impaired degradation and increased synthesis of fatty acids and, therefore, it would be interesting to analyze metabolic flux. The remodeled energy metabolism could be possibly affected through diet. Despite the remodeling of major metabolic pathways and reduced amount of mitochondria, ATP levels were normal, underlining that energy, or the lack of it, is not key in all mitochondrial diseases.

# References


Alberts, B., Johnson, A., Lewis, J., Raff, M., Roberts, K. and Walter, P. (2002), *Molecular Biology of the Cell*, 4 edn, Garland Science.

Anderson, S., Bankier, A. T., Barrell, B. G., de Bruijn, M. H., Coulson, A. R., Drouin, J., Eperon, I. C., Nierlich, D. P., Roe, B. A., Sanger, F., Schreier, P. H., Smith, A. J., Staden, R. and Young, I. G. (1981), 'Sequence and organization of the human mitochondrial genome', *Nature* **290**(5806), 457–465.

Bao, X. R., Ong, S. E., Goldberger, O., Peng, J., Sharma, R., Thompson, D. A., Vafai, S. B., Cox, A. G., Marutani, E., Ichinose, F., Goessling, W., Regev, A., Carr, S. A., Clish, C. B. and Mootha, V. K. (2016), 'Mitochondrial dysfunction remodels one-carbon metabolism in human cells', *Elife* **5**.

Becker, M. A. and Kim, M. (1987), 'Regulation of purine synthesis de novo in human fibroblasts by purine nucleotides and phosphoribosylpyrophosphate', *J. Biol. Chem.* **262**(30), 14531–14537.

Belanger, M., Allaman, I. and Magistretti, P. J. (2011), 'Brain energy metabolism: focus on astrocyte-neuron metabolic cooperation', *Cell Metab.* **14**(6), 724–738.

Boone, A. N., Chan, A., Kulpa, J. E. and Brownsey, R. W. (2000), 'Bimodal activation of acetyl-CoA carboxylase by glutamate', *J. Biol. Chem.* **275**(15), 10819–10825.

Brose, S. A., Marquardt, A. L. and Golovko, M. Y. (2014), 'Fatty acid biosynthesis from glutamate and glutamine is specifically induced in neuronal cells under hypoxia', *J. Neurochem.* **129**(3), 400–412.

Busanello, E. N., Zanatta, A., Tonin, A. M., Viegas, C. M., Vargas, C. R., Leipnitz, G., Ribeiro, C. A. and Wajner, M. (2013), 'Marked inhibition of Na+, K(+)- ATPase activity and the respiratory chain by phytanic acid in cerebellum from young rats: possible underlying mechanisms of cerebellar ataxia in Refsum disease', *J. Bioenerg. Biomembr.* **45**(1-2), 137–144.

Canto, C., Jiang, L. Q., Deshmukh, A. S., Mataki, C., Coste, A., Lagouge, M., Zierath, J. R. and Auwerx, J. (2010), 'Interdependence of AMPK and SIRT1 for metabolic adaptation to fasting and exercise in skeletal muscle', *Cell Metab.* **11**(3), 213–219.

Carling, D., Mayer, F. V., Sanders, M. J. and Gamblin, S. J. (2011), 'AMP-activated protein kinase: nature's energy sensor', *Nat. Chem. Biol.* **7**(8), 512–518.

Carling, D., Zammit, V. A. and Hardie, D. G. (1987), 'A common bicyclic protein kinase cascade inactivates the regulatory enzymes of fatty acid and cholesterol biosynthesis', *FEBS Lett.* **223**(2), 217–222.

Caviness, V. S., Takahashi, T. and Nowakowski, R. S. (1995), 'Numbers, time and neocortical neurogenesis: a general developmental and evolutionary model', *Trends Neurosci.* **18**(9), 379–383.

Chambers, S. M., Fasano, C. A., Papapetrou, E. P., Tomishima, M., Sadelain, M. and Studer, L. (2009), 'Highly efficient neural conversion of human ES and iPS cells by dual inhibition of SMAD signaling', *Nat. Biotechnol.* **27**(3), 275–280.

Chen, H. and Chan, D. C. (2009), 'Mitochondrial dynamics–fusion, fission, movement, and mitophagy–in neurodegenerative diseases', *Hum. Mol. Genet.* **18**(R2), R169–176.

Clayton, D. A. (1982), 'Replication of animal mitochondrial DNA', *Cell* **28**(4), 693–705.

Cracan, V., Titov, D. V., Shen, H., Grabarek, Z. and Mootha, V. K. (2017), 'A genetically encoded tool for manipulation of NADP+/NADPH in living cells', *Nat. Chem. Biol.* **13**(10), 1088–1095.

Csordas, G., Varnai, P., Golenar, T., Roy, S., Purkins, G., Schneider, T. G., Balla, T. and Hajnoczky, G. (2010), 'Imaging interorganelle contacts and local calcium dynamics at the ER-mitochondrial interface', *Mol. Cell* **39**(1), 121–132.

Cutler, R. G., Pedersen, W. A., Camandola, S., Rothstein, J. D. and Mattson, M. P. (2002), 'Evidence that accumulation of ceramides and cholesterol esters mediates oxidative stress-induced death of motor neurons in amyotrophic lateral sclerosis', *Ann. Neurol.* **52**(4), 448–457.

Dalton, L. E., Healey, E., Irving, J. and Marciniak, S. J. (2012), 'Phosphoproteins in stress-induced disease', *Prog Mol Biol Transl Sci* **106**, 189–221.

Dehmelt, L. and Halpain, S. (2005), 'The MAP2/Tau family of microtubule-associated proteins', *Genome Biol.* **6**(1), 204.

Delettre, C., Lenaers, G., Griffoin, J. M., Gigarel, N., Lorenzo, C., Belenguer, P., Pelloquin, L., Grosgeorge, J., Turc-Carel, C., Perret, E., Astarie-Dequeker, C., Lasquellec, L., Arnaud, B., Ducommun, B., Kaplan, J. and Hamel, C. P. (2000), 'Nuclear gene OPA1, encoding a mitochondrial dynamin-related protein, is mutated in dominant optic atrophy', *Nat. Genet.* **26**(2), 207–210.

Dimos, J. T., Rodolfa, K. T., Niakan, K. K., Weisenthal, L. M., Mitsumoto, H., Chung, W., Croft, G. F., Saphier, G., Leibel, R., Goland, R., Wichterle, H., Henderson, C. E. and Eggan, K. (2008), 'Induced pluripotent stem cells generated from patients with ALS can be differentiated into motor neurons', *Science* **321**(5893), 1218–1221.

Ducker, G. S. and Rabinowitz, J. D. (2017), 'One-Carbon Metabolism in Health and Disease', *Cell Metab.* **25**(1), 27–42.

Dudek, J., Rehling, P. and van der Laan, M. (2013), 'Mitochondrial protein import: common principles and physiological networks', *Biochim. Biophys. Acta* **1833**(2), 274–285.

Ekstrand, M. I., Falkenberg, M., Rantanen, A., Park, C. B., Gaspari, M., Hultenby, K., Rustin, P., Gustafsson, C. M. and Larsson, N. G. (2004), 'Mitochondrial transcription factor A regulates mtDNA copy number in mammals', *Hum. Mol. Genet.* **13**(9), 935–944.

El-Hattab, A. W. and Scaglia, F. (2013), 'Mitochondrial DNA depletion syndromes: review and updates of genetic basis, manifestations, and therapeutic options', *Neurotherapeutics* **10**(2), 186–198.

Erecinska, M., Cherian, S. and Silver, I. A. (2004), 'Energy metabolism in mammalian brain during development', *Prog. Neurobiol.* **73**(6), 397–445.

Fisher, R. P., Lisowsky, T., Parisi, M. A. and Clayton, D. A. (1992), 'DNA wrapping and bending by a mitochondrial high mobility group-like transcriptional activator protein', *J. Biol. Chem.* **267**(5), 3358–3367.

Florio, M. and Huttner, W. B. (2014), 'Neural progenitors, neurogenesis and the evolution of the neocortex', *Development* **141**(11), 2182–2194.

Fransen, M., Lismont, C. and Walton, P. (2017), 'The Peroxisome-Mitochondria Connection: How and Why?', *Int J Mol Sci* **18**(6).

Friedman, J. R., Lackner, L. L., West, M., DiBenedetto, J. R., Nunnari, J. and Voeltz, G. K. (2011), 'ER tubules mark sites of mitochondrial division', *Science* **334**(6054), 358–362.

Garone, C., Garcia-Diaz, B., Emmanuele, V., Lopez, L. C., Tadesse, S., Akman, H. O., Tanji, K., Quinzii, C. M. and Hirano, M. (2014), 'Deoxypyrimidine monophosphate bypass therapy for thymidine kinase 2 deficiency', *EMBO Mol Med* **6**(8), 1016–1027.

Giorgi, C., Romagnoli, A., Pinton, P. and Rizzuto, R. (2008), 'Ca2+ signaling, mitochondria and cell death', *Curr. Mol. Med.* **8**(2), 119–130.

Hakonen, A. H., Goffart, S., Marjavaara, S., Paetau, A., Cooper, H., Mattila, K., Lampinen, M., Sajantila, A., Lonnqvist, T., Spelbrink, J. N. and Suomalainen, A. (2008), 'Infantile-onset spinocerebellar ataxia and mitochondrial recessive ataxia syndrome are associated with neuronal complex I defect and mtDNA depletion', *Hum. Mol. Genet.* **17**(23), 3822–3835.

Hakonen, A. H., Isohanni, P., Paetau, A., Herva, R., Suomalainen, A. and Lonnqvist, T. (2007), 'Recessive Twinkle mutations in early onset encephalopathy with mtDNA depletion', *Brain* **130**(Pt 11), 3032–3040.

Hamalainen, R. H., Manninen, T., Koivumaki, H., Kislin, M., Otonkoski, T. and Suomalainen, A. (2013), 'Tissue- and cell-type-specific manifestations of heteroplasmic mtDNA 3243A¿G mutation in human induced pluripotent stem cell-derived disease model', *Proc. Natl. Acad. Sci. U.S.A.* **110**(38), E3622–3630.

Hamanaka, R. B. and Chandel, N. S. (2010), 'Mitochondrial reactive oxygen species regulate cellular signaling and dictate biological outcomes', *Trends Biochem. Sci.* **35**(9), 505–513.

Hardie, D. G., Hawley, S. A. and Scott, J. W. (2006), 'AMP-activated protein kinase–development of the energy sensor concept', *J. Physiol. (Lond.)* **574**(Pt 1), 7–15.

Heikkila, T. J., Yla-Outinen, L., Tanskanen, J. M., Lappalainen, R. S., Skottman, H., Suuronen, R., Mikkonen, J. E., Hyttinen, J. A. and Narkilahti, S. (2009), 'Human embryonic stem cell-derived neuronal cells form spontaneously active neuronal networks in vitro', *Exp. Neurol.* **218**(1), 109–116.

Hirsch, D., Stahl, A. and Lodish, H. F. (1998), 'A family of fatty acid transporters conserved from mycobacterium to man', *Proc. Natl. Acad. Sci. U.S.A.* **95**(15), 8625–8629.

Holt, I. J., Lorimer, H. E. and Jacobs, H. T. (2000), 'Coupled leading- and lagging-strand synthesis of mammalian mitochondrial DNA', *Cell* **100**(5), 515–524.

Hoppeler, H. and Fluck, M. (2003), 'Plasticity of skeletal muscle mitochondria: structure and function', *Med Sci Sports Exerc* **35**(1), 95–104.

Iborra, F. J., Kimura, H. and Cook, P. R. (2004), 'The functional organization of mitochondrial genomes in human cells', *BMC Biol.* **2**, 9.

Israel, M. A., Yuan, S. H., Bardy, C., Reyna, S. M., Mu, Y., Herrera, C., Hefferan, M. P., Van Gorp, S., Nazor, K. L., Boscolo, F. S., Carson, C. T., Laurent, L. C., Marsala, M., Gage, F. H., Remes, A. M., Koo, E. H. and Goldstein, L. S. (2012), 'Probing sporadic and familial Alzheimer's disease using induced pluripotent stem cells', *Nature* **482**(7384), 216–220.

Jeon, I., Lee, N., Li, J. Y., Park, I. H., Park, K. S., Moon, J., Shim, S. H., Choi, C., Chang, D. J., Kwon, J., Oh, S. H., Shin, D. A., Kim, H. S., Do, J. T., Lee, D. R., Kim, M., Kang, K. S., Daley, G. Q., Brundin, P. and Song, J. (2012), 'Neuronal properties, in vivo effects, and pathology of a Huntington's disease patient-derived induced pluripotent stem cells', *Stem Cells* **30**(9), 2054–2062.

Kann, O. and Kovacs, R. (2007), 'Mitochondria and neuronal activity', *Am. J. Physiol., Cell Physiol.* **292**(2), C641–657.

Kim, I., Rodriguez-Enriquez, S. and Lemasters, J. J. (2007), 'Selective degradation of mitochondria by mitophagy', *Arch. Biochem. Biophys.* **462**(2), 245–253.

Klingerberg, M. and Buecher, T. (1960), 'Biological oxidations', *Annu. Rev. Biochem.* **29**, 669–708.

Korhonen, J. A., Pham, X. H., Pellegrini, M. and Falkenberg, M. (2004), 'Reconstitution of a minimal mtDNA replisome in vitro', *EMBO J.* **23**(12), 2423–2429.

Koskinen, T., Santavuori, P., Sainio, K., Lappi, M., Kallio, A. K. and Pihko, H. (1994), 'Infantile onset spinocerebellar ataxia with sensory neuropathy: a new inherited disease', *J. Neurol. Sci.* **121**(1), 50–56.

Lane, N. and Martin, W. (2010), 'The energetics of genome complexity', *Nature* **467**(7318), 929–934.

Lappalainen, R. S., Salomaki, M., Yla-Outinen, L., Heikkila, T. J., Hyttinen, J. A., Pihlajamaki, H., Suuronen, R., Skottman, H. and Narkilahti, S. (2010), 'Similarly derived and cultured hESC lines show variation in their developmental potential towards neuronal cells in long-term culture', *Regen Med* **5**(5), 749–762.

Lewis, S. C., Uchiyama, L. F. and Nunnari, J. (2016), 'ER-mitochondria contacts couple mtDNA synthesis with mitochondrial division in human cells', *Science* **353**(6296), aaf5549.

Ligon, L. A. and Steward, O. (2000), 'Movement of mitochondria in the axons and dendrites of cultured hippocampal neurons', *J. Comp. Neurol.* **427**(3), 340–350.

Lill, R. and Kispal, G. (2000), 'Maturation of cellular Fe-S proteins: an essential function of mitochondria', *Trends Biochem. Sci.* **25**(8), 352–356.

Lim, S. C., Tajika, M., Shimura, M., Carey, K. T., Stroud, D. A., Murayama, K., Ohtake, A. and McKenzie, M. (2018), 'Loss of the Mitochondrial Fatty Acid B-Oxidation Protein Medium-Chain Acyl-Coenzyme A Dehydrogenase Disrupts Oxidative Phosphorylation Protein Complex Stability and Function', *Sci Rep* **8**(1), 153.

Longley, M. J., Ropp, P. A., Lim, S. E. and Copeland, W. C. (1998), 'Characterization of the native and recombinant catalytic subunit of human DNA polymerase gamma: identification of residues critical for exonuclease activity and dideoxynucleotide sensitivity', *Biochemistry* **37**(29), 10529–10539.

Lu, C. and Thompson, C. B. (2012), 'Metabolic regulation of epigenetics', *Cell Metab.* **16**(1), 9–17.

McWilliams, T. G., Prescott, A. R., Allen, G. F., Tamjar, J., Munson, M. J., Thomson, C., Muqit, M. M. and Ganley, I. G. (2016), 'mito-QC illuminates mitophagy and mitochondrial architecture in vivo', *J. Cell Biol.* **214**(3), 333–345.

Menzies, R. A. and Gold, P. H. (1971), 'The turnover of mitochondria in a variety of tissues of young adult and aged rats', *J. Biol. Chem.* **246**(8), 2425–2429.

Mertens, J., Marchetto, M. C., Bardy, C. and Gage, F. H. (2016), 'Evaluating cell reprogramming, differentiation and conversion technologies in neuroscience', *Nat. Rev. Neurosci.* **17**(7), 424–437.

Mitchell, P. (1961), 'Coupling of phosphorylation to electron and hydrogen transfer by a chemi-osmotic type of mechanism', *Nature* **191**, 144–148.

Muller, F. L., Liu, Y. and Van Remmen, H. (2004), 'Complex III releases superoxide to both sides of the inner mitochondrial membrane', *J. Biol. Chem.* **279**(47), 49064–49073.

Munday, M. R. (2002), 'Regulation of mammalian acetyl-CoA carboxylase', *Biochem. Soc. Trans.* **30**(Pt 6), 1059–1064.

Murphy, M. P. (2009), 'How mitochondria produce reactive oxygen species', *Biochem. J.* **417**(1), 1–13.

Neupert, W. and Herrmann, J. M. (2007), 'Translocation of proteins into mitochondria', *Annu. Rev. Biochem.* **76**, 723–749.

Niedzielska, E., Smaga, I., Gawlik, M., Moniczewski, A., Stankowicz, P., Pera, J. and Filip, M. (2016), 'Oxidative Stress in Neurodegenerative Diseases', *Mol. Neurobiol.* **53**(6), 4094–4125.

Nikali, K., Suomalainen, A., Saharinen, J., Kuokkanen, M., Spelbrink, J. N., Lonnqvist, T. and Peltonen, L. (2005), 'Infantile onset spinocerebellar ataxia is caused by recessive mutations in mitochondrial proteins Twinkle and Twinky', *Hum. Mol. Genet.* **14**(20), 2981–2990.

Nikkanen, J., Forsstrom, S., Euro, L., Paetau, I., Kohnz, R. A., Wang, L., Chilov, D., Viinamaki, J., Roivainen, A., Marjamaki, P., Liljenback, H., Ahola, S., Buzkova, J., Terzioglu, M., Khan, N. A.,

Pirnes-Karhu, S., Paetau, A., Lonnqvist, T., Sajantila, A., Isohanni, P., Tyynismaa, H., Nomura, D. K., Battersby, B. J., Velagapudi, V., Carroll, C. J. and Suomalainen, A. (2016), 'Mitochondrial DNA Replication Defects Disturb Cellular dNTP Pools and Remodel One-Carbon Metabolism', *Cell Metab.* **23**(4), 635–648.

Nsiah-Sefaa, A. and McKenzie, M. (2016), 'Combined defects in oxidative phosphorylation and fatty acid $\beta$-oxidation in mitochondrial disease', *Biosci. Rep.* **36**(2).

Nunnari, J. and Suomalainen, A. (2012), 'Mitochondria: in sickness and in health', *Cell* **148**(6), 1145–1159.

Pilz, R. B., Willis, R. C. and Boss, G. R. (1984), 'The influence of ribose 5-phosphate availability on purine synthesis of cultured human lymphoblasts and mitogen-stimulated lymphocytes', *J. Biol. Chem.* **259**(5), 2927–2935.

Pohjoismaki, J. L., Goffart, S., Tyynismaa, H., Willcox, S., Ide, T., Kang, D., Suomalainen, A., Karhunen, P. J., Griffith, J. D., Holt, I. J. and Jacobs, H. T. (2009), 'Human heart mitochondrial DNA is organized in complex catenated networks containing abundant four-way junctions and replication forks', *J. Biol. Chem.* **284**(32), 21446–21457.

Qi, X., Lewin, A. S., Hauswirth, W. W. and Guy, J. (2003), 'Optic neuropathy induced by reductions in mitochondrial superoxide dismutase', *Invest. Ophthalmol. Vis. Sci.* **44**(3), 1088–1096.

Quiros, P. M., Mottis, A. and Auwerx, J. (2016), 'Mitonuclear communication in homeostasis and stress', *Nat. Rev. Mol. Cell Biol.* **17**(4), 213–226.

Ring, K. L., Tong, L. M., Balestra, M. E., Javier, R., Andrews-Zwilling, Y., Li, G., Walker, D., Zhang, W. R., Kreitzer, A. C. and Huang, Y. (2012), 'Direct reprogramming of mouse and human fibroblasts into multipotent neural stem cells with a single factor', *Cell Stem Cell* **11**(1), 100–109.

Rugarli, E. I. and Langer, T. (2012), 'Mitochondrial quality control: a matter of life and death for neurons', *EMBO J.* **31**(6), 1336–1349.

Sanchez-Danes, A., Richaud-Patin, Y., Carballo-Carbajal, I., Jimenez-Delgado, S., Caig, C., Mora, S., Di Guglielmo, C., Ezquerra, M., Patel, B., Giralt, A., Canals, J. M., Memo, M., Alberch, J., Lopez-Barneo, J., Vila, M., Cuervo, A. M., Tolosa, E., Consiglio, A. and Raya, A. (2012), 'Disease-specific phenotypes in dopamine neurons from human iPS-based models of genetic and sporadic Parkinson's disease', *EMBO Mol Med* **4**(5), 380–395.

Saraste, M. (1999), 'Oxidative phosphorylation at the fin de sicle', *Science* **283**(5407), 1488–1493.

Schagger, H. and Pfeiffer, K. (2000), 'Supercomplexes in the respiratory chains of yeast and mammalian mitochondria', *EMBO J.* **19**(8), 1777–1783.

Shi, Y., Dierckx, A., Wanrooij, P. H., Wanrooij, S., Larsson, N. G., Wilhelmsson, L. M., Falkenberg, M. and Gustafsson, C. M. (2012a), 'Mammalian transcription factor A is a core component of the mitochondrial transcription machinery', *Proc. Natl. Acad. Sci. U.S.A.* **109**(41), 16510–16515.

Shi, Y., Kirwan, P., Smith, J., Robinson, H. P. and Livesey, F. J. (2012b), 'Human cerebral cortex development from pluripotent stem cells to functional excitatory synapses', *Nat. Neurosci.* **15**(3), 477–486.

Smirnova, E., Griparic, L., Shurland, D. L. and van der Bliek, A. M. (2001), 'Dynamin-related protein Drp1 is required for mitochondrial division in mammalian cells', *Mol. Biol. Cell* **12**(8), 2245–2256.

Song, Z., Ghochani, M., McCaffery, J. M., Frey, T. G. and Chan, D. C. (2009), 'Mitofusins and OPA1 mediate sequential steps in mitochondrial membrane fusion', *Mol. Biol. Cell* **20**(15), 3525–3532.

Spelbrink, J. N., Li, F. Y., Tiranti, V., Nikali, K., Yuan, Q. P., Tariq, M., Wanrooij, S., Garrido, N., Comi, G., Morandi, L., Santoro, L., Toscano, A., Fabrizi, G. M., Somer, H., Croxen, R., Beeson, D., Poulton, J., Suomalainen, A., Jacobs, H. T., Zeviani, M. and Larsson, C. (2001), 'Human mitochondrial DNA deletions associated with mutations in the gene encoding Twinkle, a phage T7 gene 4-like protein localized in mitochondria', *Nat. Genet.* **28**(3), 223–231.

Suomalainen, A. and Battersby, B. J. (2017), 'Mitochondrial diseases: the contribution of organelle stress responses to pathology', *Nat. Rev. Mol. Cell Biol.* .

Suomalainen, A. and Isohanni, P. (2010), 'Mitochondrial DNA depletion syndromes–many genes, common mechanisms', *Neuromuscul. Disord.* **20**(7), 429–437.

Takahashi, K. and Yamanaka, S. (2006), 'Induction of pluripotent stem cells from mouse embryonic and adult fibroblast cultures by defined factors', *Cell* **126**(4), 663–676.

Tibbetts, A. S. and Appling, D. R. (2010), 'Compartmentalization of Mammalian folate-mediated one-carbon metabolism', *Annu. Rev. Nutr.* **30**, 57–81.

Timmis, J. N., Ayliffe, M. A., Huang, C. Y. and Martin, W. (2004), 'Endosymbiotic gene transfer: organelle genomes forge eukaryotic chromosomes', *Nat. Rev. Genet.* **5**(2), 123–135.

Titov, D. V., Cracan, V., Goodman, R. P., Peng, J., Grabarek, Z. and Mootha, V. K. (2016), 'Complementation of mitochondrial electron transport chain by manipulation of the NAD+/NADH ratio', *Science* **352**(6282), 231–235.

Tortora, G. J. and Derrickson, B. (2012), *Principles of Anatomy and Physiology*, 13 edn, John Wiley and Sons, Inc.

Touma, E. H. and Charpentier, C. (1992), 'Medium chain acyl-CoA dehydrogenase deficiency', *Arch. Dis. Child.* **67**(1), 142–145.

Tserng, K. Y., Jin, S. J., Kerr, D. S. and Hoppel, C. L. (1990), 'Abnormal urinary excretion of unsaturated dicarboxylic acids in patients with medium-chain acyl-CoA dehydrogenase deficiency', *J. Lipid Res.* **31**(5), 763–771.

Turrens, J. F. (2003), 'Mitochondrial formation of reactive oxygen species', *J. Physiol. (Lond.)* **552**(Pt 2), 335–344.

Tyynismaa, H., Carroll, C. J., Raimundo, N., Ahola-Erkkila, S., Wenz, T., Ruhanen, H., Guse, K., Hemminki, A., Peltola-Mj?sund, K. E., Tulkki, V., Oresic, M., Moraes, C. T., Pietilainen, K., Hovatta, I. and Suomalainen, A. (2010), 'Mitochondrial myopathy induces a starvation-like response', *Hum. Mol. Genet.* **19**(20), 3948–3958.

Tyynismaa, H., Sembongi, H., Bokori-Brown, M., Granycome, C., Ashley, N., Poulton, J., Jalanko, A., Spelbrink, J. N., Holt, I. J. and Suomalainen, A. (2004), 'Twinkle helicase is essential for mtDNA maintenance and regulates mtDNA copy number', *Hum. Mol. Genet.* **13**(24), 3219–3227.

Vagelos, P. R., Alberts, A. W. and Martin, D. B. (1963), 'Studies on the mechnism of activation of acetyl coenzyme A carboxylase by citrate', *J. Biol. Chem.* **238**, 533–540.

Valentine, J. S. and Hart, P. J. (2003), 'Misfolded CuZnSOD and amyotrophic lateral sclerosis', *Proc. Natl. Acad. Sci. U.S.A.* **100**(7), 3617–3622.

Vierbuchen, T., Ostermeier, A., Pang, Z. P., Kokubu, Y., Sudhof, T. C. and Wernig, M. (2010), 'Direct conversion of fibroblasts to functional neurons by defined factors', *Nature* **463**(7284), 1035–1041.

Wang, Y., Mohsen, A. W., Mihalik, S. J., Goetzman, E. S. and Vockley, J. (2010), 'Evidence for physical association of mitochondrial fatty acid oxidation and oxidative phosphorylation complexes', *J. Biol. Chem.* **285**(39), 29834–29841.

Williams, E. G., Wu, Y., Jha, P., Dubuis, S., Blattmann, P., Argmann, C. A., Houten, S. M., Amariuta, T., Wolski, W., Zamboni, N., Aebersold, R. and Auwerx, J. (2016), 'Systems proteomics of liver mitochondria function', *Science* **352**(6291), aad0189.

Wonders, C. P. and Anderson, S. A. (2006), 'The origin and specification of cortical interneurons', *Nat. Rev. Neurosci.* **7**(9), 687–696.

Wu, Z., Puigserver, P., Andersson, U., Zhang, C., Adelmant, G., Mootha, V., Troy, A., Cinti, S., Lowell, B., Scarpulla, R. C. and Spiegelman, B. M. (1999), 'Mechanisms controlling mitochondrial biogenesis and respiration through the thermogenic coactivator PGC-1', *Cell* **98**(1), 115–124.

Xia, G., Santostefano, K., Hamazaki, T., Liu, J., Subramony, S. H., Terada, N. and Ashizawa, T. (2013), 'Generation of human-induced pluripotent stem cells to model spinocerebellar ataxia type 2 in vitro', *J. Mol. Neurosci.* **51**(2), 237–248.

Xia, J. and Wishart, D. S. (2016), 'Using MetaboAnalyst 3.0 for Comprehensive Metabolomics Data Analysis', *Curr Protoc Bioinformatics* **55**, 1–14.

Yakubovskaya, E., Chen, Z., Carrodeguas, J. A., Kisker, C. and Bogenhagen, D. F. (2006), 'Functional human mitochondrial DNA polymerase gamma forms a heterotrimer', *J. Biol. Chem.* **281**(1), 374–382.

Yang, M. Y., Bowmaker, M., Reyes, A., Vergani, L., Angeli, P., Gringeri, E., Jacobs, H. T. and Holt, I. J. (2002), 'Biased incorporation of ribonucleotides on the mitochondrial L-strand accounts for apparent strand-asymmetric DNA replication', *Cell* **111**(4), 495–505.

Yang, S. Y., He, X. Y. and Schulz, H. (1987), 'Fatty acid oxidation in rat brain is limited by the low activity of 3-ketoacyl-coenzyme A thiolase', *J. Biol. Chem.* **262**(27), 13027–13032.

Yasukawa, T., Reyes, A., Cluett, T. J., Yang, M. Y., Bowmaker, M., Jacobs, H. T. and Holt, I. J. (2006), 'Replication of vertebrate mitochondrial DNA entails transient ribonucleotide incorporation throughout the lagging strand', *EMBO J.* **25**(22), 5358–5371.

Ying, W. (2008), 'NAD+/NADH and NADP+/NADPH in cellular functions and cell death: regulation and biological consequences', *Antioxid. Redox Signal.* **10**(2), 179–206.

Yoo, A. S., Sun, A. X., Li, L., Shcheglovitov, A., Portmann, T., Li, Y., Lee-Messer, C., Dolmetsch, R. E., Tsien, R. W. and Crabtree, G. R. (2011), 'MicroRNA-mediated conversion of human fibroblasts to neurons', *Nature* **476**(7359), 228–231.

Zhang, X., Huang, C. T., Chen, J., Pankratz, M. T., Xi, J., Li, J., Yang, Y., Lavaute, T. M., Li, X. J., Ayala, M., Bondarenko, G. I., Du, Z. W., Jin, Y., Golos, T. G. and Zhang, S. C. (2010), 'Pax6 is a human neuroectoderm cell fate determinant', *Cell Stem Cell* **7**(1), 90–100.

Zuchner, S., Mersiyanova, I. V., Muglia, M., Bissar-Tadmouri, N., Rochelle, J., Dadali, E. L., Zappia, M., Nelis, E., Patitucci, A., Senderek, J., Parman, Y., Evgrafov, O., Jonghe, P. D., Takahashi, Y., Tsuji, S., Pericak-Vance, M. A., Quattrone, A., Battaloglu, E., Polyakov, A. V., Timmerman, V., Schroder, J. M., Vance, J. M. and Battologlu, E. (2004), 'Mutations in the mitochondrial GTPase mitofusin 2 cause Charcot-Marie-Tooth neuropathy type 2A', *Nat. Genet.* **36**(5), 449–451.